

Chapter 5

Neutrino Experiments

J.M. Conrad

*Department of Physics,
Columbia University,
New York, NY*

This article is a summary of four introductory lectures on “Neutrino Experiments,” given at the 2006 TASI summer school. The purpose was to sketch out the present questions in neutrino physics, and discuss the experiments that can address them. The ideas were then explored in depth by later lecturers.

This article begins with an overview of neutrinos in the Standard Model and what we know about these particles today. This is followed by a discussion of the direction of the field, divided into the three themes identified in the *APS Study on the Future of Neutrino Physics*.¹ This APS study represented the culmination of a year-long effort by the neutrino community to come to a consensus on future directions. The report is recommended reading for students, along with the accompanying working group white papers, especially the Theory Group Whitepaper.²

While these lectures used the APS Neutrino Study themes as the core, the emphasis here is different from the APS report. The point of a summer school is to teach specific ideas rather than provide a perfectly balanced overview of the field. The result is that, with apologies, some experiments were necessarily left out of the discussion. Students are referred to the Neutrino Oscillation Industry Website³ for a complete list of all neutrino experiments, by category.

5.1. Neutrinos As We Knew Them

Neutrinos are different from the other fermions. Even before the recent evidence of neutrino mass, neutrinos were peculiar members of the Standard

Model. They are the only fermions

- to carry no electric charge.
- for which we have no evidence of a right-handed partner.
- that are defined as massless.

These ideas are connected by the fact that, unlike other spin 1/2 particles, neutrinos can only interact through the weak interaction.

Even though the Standard Model picture is now demonstrably wrong, this theoretical framework provides a good place to start the discussion. This section begins by expanding on the Standard Model picture of the neutrino sketched above. It then discusses how neutrinos interact. This is followed by an overview of neutrino sources and detectors.

5.1.1. *Neutrinos in the Standard Model*

Neutrinos are the only Standard Model fermions to interact strictly via the weak interaction. This proceeds through two types of boson exchange. Exchange of the Z^0 is called the neutral current (NC) interaction. Exchange of the W^\pm is called the charged current (CC) interaction. When a W is emitted, charge conservation at the vertex requires that a charged lepton exits the interaction. We know the family of an incoming neutrino by the charged partner which exits the CC interaction. For example, a scattered electron tags a ν_e interaction, a μ tags a ν_μ interaction, and a τ tags a ν_τ interaction. The neutrino always emits the W^+ and the antineutrino always emits the W^- in the CC interaction. In order to conserve charge at the lower vertex, the CC interaction is flavor-changing for target quarks. For example, in a neutrino interaction, if a neutron, n , absorbs a W^+ , a proton, p , will exit the interaction. The W has converted a d quark to a u quark. The first two diagrams shown on Fig. 5.1 illustrate a NC and a CC interaction, respectively.

In 1989, measurements of the Z^0 width at LEP⁴ and SLD⁵ determined that there are only three families of light-mass weakly-interacting neutrinos, although we will explore this question in more depth in section 3 of these lectures. These are the ν_e , the ν_μ , and the ν_τ . The interactions of the ν_e and ν_μ have been shown to be consistent with the Standard Model weak interaction. Until recently, there has only been indirect evidence for the ν_τ through the decay of the τ meson. In July 2000, however, the DoNuT Experiment (E872) at Fermilab presented direct evidence for ν_τ interactions.⁶

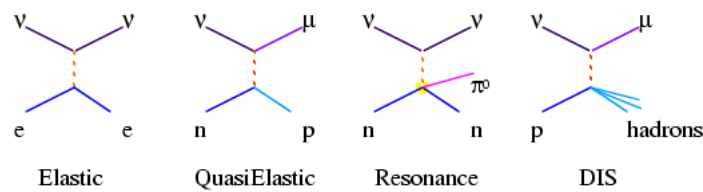


Fig. 5.1. Examples of the four types of neutrino interactions which appear throughout this discussion and are defined in sec. 5.1.2. The first two diagrams show an NC and CC interaction, respectively.

Within the Standard Model, neutrinos are massless. This assumption is consistent with direct experimental observation. It is also an outcome of the feature of “handedness” associated with neutrinos. To understand handedness, it is simplest to begin by discussing “helicity,” since for massless particles helicity and handedness are identical.

For a spin $1/2$ Dirac particle, helicity is the projection of a particle’s spin (Σ) along its direction of motion $\hat{\mathbf{p}}$, with operator $\Sigma \cdot \hat{\mathbf{p}}$. Helicity has two possible states: spin aligned opposite the direction of motion (negative, or “left helicity”) and spin aligned along the direction of motion (positive or “right helicity”). If a particle is massive, then the sign of the helicity of the particle will be frame dependent. When one boosts to a frame where one is moving faster than the particle, the sign of the momentum will change but the spin will not, and therefore the helicity will flip. For massless particles, which must travel at the speed of light, one cannot boost to a frame where helicity changes sign.

Handedness (or chirality) is the Lorentz invariant (*i.e.*, frame-independent) analogue of helicity for both massless and massive Dirac particles. There are two states: “left handed” (LH) and “right handed” (RH). For the case of massless particles, including Standard Model neutrinos, helicity and handedness are identical. A massless fermion is either purely LH or RH, and, in principle, can appear in either state. Massive particles have both RH and LH components. A helicity eigenstate for a massive particle is a combination of handedness states. It is only in the high en-

ergy limit, where particles are effectively massless, that handedness and helicity coincide for massive fermions. Nevertheless, people tend to use the terms “helicity” and “handedness” interchangeably. Unlike the electromagnetic and strong interactions, the weak interaction involving neutrinos has a definite preferred handedness.

In 1956, it was shown that neutrinos are LH and outgoing antineutrinos are RH.⁷ This effect is called “parity violation.” If neutrinos respected parity, then an equal number of LH and RH neutrinos should have been produced in the 1956 experiment. The fact that all neutrinos are LH and all antineutrinos are RH means that, unlike all of the other fermions in the Standard Model, parity appears to be maximally violated for this particle. This is clearly very strange.

We need a method to enforce parity violation within the weak interaction theory. To this end, consider a fermion wavefunction, ψ , broken up into its LH and RH components:

$$\psi = \psi_L + \psi_R. \quad (5.1)$$

We can introduce a projection operator which selects out each component:

$$\gamma^5 \psi_{L,R} = \mp \psi_{L,R}. \quad (5.2)$$

To force the correct handedness in calculations involving the weak interaction, we can require a factor of $(1 - \gamma^5)/2$ at every weak vertex involving a neutrino. As a result of this factor, which corresponds to the LH projection operator, we often say the charged weak interaction (W exchange) is “left handed.”

Note that by approaching the problem this way, RH neutrinos (and LH antineutrinos) could in principle exist but be undetected because they do not interact. They will not interact via the electromagnetic interactions because they are neutral, or via the strong interaction because they are leptons. RH Dirac neutrinos do not couple to the Standard Model W , because this interaction is “left handed,” as discussed above. Because they are non-interacting, they are called “sterile neutrinos.” By definition, the Standard Model has no RH neutrino.

With no RH partner, the neutrino can have no Dirac mass term in the Lagrangian. To see this, note that the free-particle Lagrangian for a massive, spin 1/2 particle is

$$\mathcal{L} = i\bar{\psi}\gamma_\mu\partial^\mu\psi - m\bar{\psi}\psi, \quad (5.3)$$

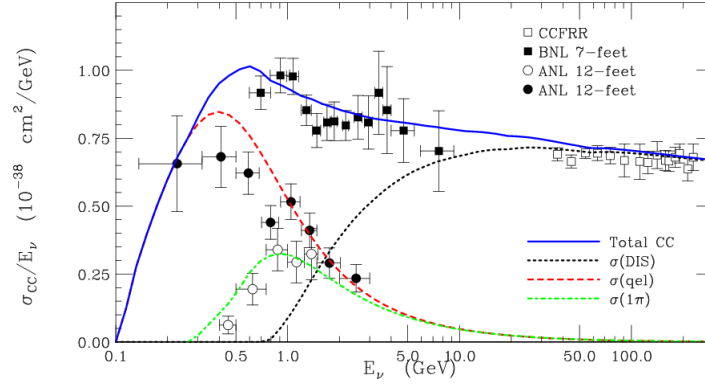


Fig. 5.2. Current status of ν_μ CC cross section measurements in the 1 to 100 GeV range. This plot shows σ/E , thus removing the linear energy dependence at high energies. Note the low energy cut-off due to the muon mass suppression. Components of the total cross section are indicated by the curves.⁸

However, $\bar{\psi}\psi$ can be rewritten using

$$\psi_{L,R} = 1/2(1 \mp \gamma^5)\psi, \quad (5.4)$$

$$\bar{\psi}_{L,R} = 1/2\bar{\psi}(1 \pm \gamma^5), \quad (5.5)$$

giving

$$\bar{\psi}\psi = \bar{\psi} \left[\frac{1 + \gamma^5}{2} + \frac{1 - \gamma^5}{2} \right] \left[\frac{1 + \gamma^5}{2} + \frac{1 - \gamma^5}{2} \right] \psi = \bar{\psi}_L \psi_R + \bar{\psi}_R \psi_L. \quad (5.6)$$

In other words, an $m\bar{\psi}\psi$ (“mass”) term in a Lagrangian mixes RH and LH states of the fermion. If the fermions have only one handedness (like ν_s), then the Dirac mass term will automatically vanish. In the Standard Model, there is no Dirac mass term for neutrinos.

5.1.2. Neutrino Interactions

Neutrino interactions in the Standard Model come in four basic types. Fig. 5.1 shows examples of the four interactions. In *Elastic* scattering, “what goes is what comes out,” just like two billiard balls colliding. An example is a NC interaction where the target does not go into an excited state or break up, *e.g.*, $\nu_e + n \rightarrow \nu_e + n$. A more complicated example is electron-neutrino scattering from electrons, where the W exchange yields

a final state which is indistinguishable from the Z exchange on an event-by-event basis, so this is categorized as an elastic scatter. *Quasi-elastic* scattering is, generally, the CC analogue to elastic scattering. Exchange of the W causes the incoming lepton and the target to change flavors, but the target does not go into an excited state or break apart. An example is $\nu_\mu + n \rightarrow \mu + p$. *Single pion* production may be caused by either NC or CC interactions. In resonant single pion production, the target becomes a Δ which decays to emit a pion. In coherent scattering, there is little momentum exchange with the nucleon and a single pion is produced diffractively in the forward direction. The case of NC single π^0 production is particularly important, because this forms a background in many neutrino oscillation searches. Finally, *DIS*, or Deep Inelastic Scattering, is the case where there is large 4-momentum exchange, breaking the nucleon apart. One can have NC or CC deep inelastic scattering.

Fig. 5.2 summarizes the low energy behavior of σ/E for CC events (solid line), as predicted by the NUANCE neutrino event generator.⁹ The quasi-elastic, single pion and deep inelastic contributions are indicated by the broken curves. The data indicate the state of the art for neutrino cross section measurements. One can see that if precision neutrino studies are to be pursued in the MeV to few GeV range, that more accurate measurements are essential. The MiniBooNE,¹⁰ SciBooNE,¹¹ and MINERvA¹² experiments are expected to improve the situation in the near future.

Above a few GeV, the total neutrino cross section rises linearly with energy. The total cross section is the sum of many partial cross sections: quasi-elastic + single pion + two pions + three pions + etc. As the energy increases, each of these cross sections sequentially “turns on” and then becomes constant with energy. Thus the sum, which is the total cross section, increases continuously and linearly with E .

Nevertheless, even at high energies, this interaction is called “weak” for good reason. The total cross section for most neutrino scattering experiments is small. For 100 GeV ν_μ interactions with electrons, the cross section is $\sim 10^{-40}$ cm². For 100 GeV ν_μ interactions with nucleons, the cross section is $\sim 10^{-36}$ cm². This is many orders of magnitude less than the strong interaction. For example, for pp scattering, the cross section is $\sim 10^{-25}$ cm². The result is that a 100 GeV neutrino will have a mean free path in iron of 3×10^9 meters. Thus most neutrinos which hit the Earth travel through without interacting. It is only at ultra-high energies that the Earth becomes opaque to neutrinos, as discussed in sec. 5.3.3.2.

In principle, the interactions of the ν_e , ν_μ , and ν_τ should be identical

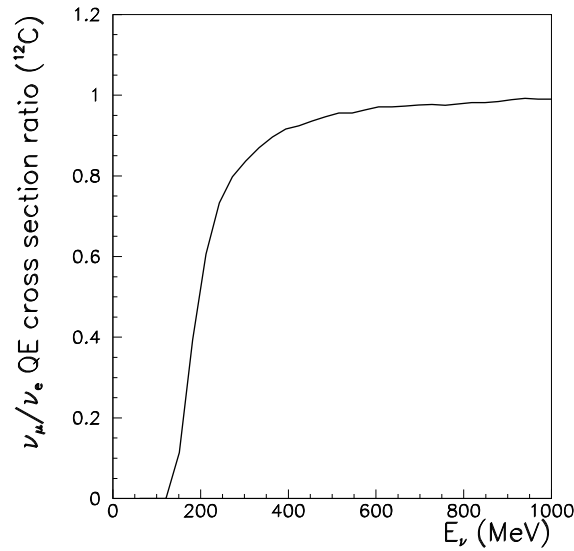


Fig. 5.3. The ratio of the ν_e to ν_μ CC cross sections as a function of neutrino energy, showing the suppression due to the lepton mass.

(“universal”). In practice, the mass differences of the outgoing leptons lead to considerable differences in the behavior of the cross sections. In the CC interaction, you must have enough CM energy to actually produce the outgoing charged lepton. Just above mass threshold, there is very little phase space for producing the lepton, and so production will be highly suppressed. The cross section increases in a non-linear manner until well above threshold. Consider, for example, a comparison of the ν_e and ν_μ CC quasielastic cross section on carbon, shown in Fig. 5.3. At very low energy the CC ν_μ cross section is zero, while the ν_e cross section is non-zero, because the 105 MeV muon cannot be produced. The ratio approaches one at about 1 GeV. A similar effect occurs for the ν_τ CC interaction cross sections. The mass of the τ is 1.8 GeV, resulting in a cross section which is zero below 3.5 GeV and suppressed relative to the total ν_μ CC scattering cross section for ν_τ beam energies beyond 100 GeV. At 100 GeV, which corresponds to a center-of-mass energy of $\sqrt{2ME} \approx 14$ GeV, there is still a 25% reduction in the total CC ν_τ interaction rate compared to ν_μ due to

leptonic mass suppression.

For low energy neutrino sources, the CC interaction may also be suppressed due to conversion of the nucleon at the lower vertex. For example, the CC interaction commonly called “inverse beta decay” (IBD), $\bar{\nu}_e p \rightarrow e^+ n$, which is crucial to reactor neutrino experiments, has a threshold of 1.084 MeV, driven by the mass difference between the proton and the neutron plus the mass of the positron. In the case of bound nuclei, the energy transferred in a CC interaction must overcome the binding energy difference between the incoming and outgoing nucleus as well as the mass suppression due to the charged lepton. This leads to nuclear-dependent thresholds for the CC interaction. For example:

$$\begin{aligned} {}^{35}\text{Cl}(75.8\%) &\rightarrow {}^{35}\text{Ar} : & 5.967 \text{ MeV}; \\ {}^{37}\text{Cl}(24.2\%) &\rightarrow {}^{37}\text{Ar} : & 0.813 \text{ MeV}; \\ {}^{69}\text{Ga}(60.1\%) &\rightarrow {}^{69}\text{Ge} : & 2.227 \text{ MeV}; \\ {}^{71}\text{Ga}(39.9\%) &\rightarrow {}^{71}\text{Ge} : & 0.232 \text{ MeV}. \end{aligned}$$

are the thresholds for isotopes which have been used as targets in past solar neutrino (ν_e) detectors.^{14–16}

In discussing neutrino scattering at higher energies, several kinematic quantities are used to describe events. The squared center of mass energy is represented by the Mandelstam variable, s . The energy transferred by the boson is ν , and $y = \nu/E_\nu$ is the fractional energy transfer, or “inelasticity.” The distribution of events as a function of y depends on the helicity. For neutrino scattering from quarks, the y -dependence is flat, but for antineutrinos, the differential cross section is peaked at low y . The variable Q^2 is the negative squared four-momentum transfer. Deep inelastic scattering begins to occur at $Q^2 \sim 1 \text{ GeV}^2$. If x is the fractional momentum carried by a struck quark in a deep inelastic scatter, then $x = Q^2/2M\nu$, where M is the target mass. Elastic and quasielastic scattering occur at $x = 1$, hence $Q^2 = 2M\nu \approx sxy$, valid for large s .

5.1.3. Sources of Neutrinos

With such a small interaction probability, it is clear that intense neutrino sources are needed to have high statistics in a neutrino experiment. The primary sources of neutrino for interactions observed on Earth are the Sun, cosmic-ray interactions, reactors, and accelerator beams.

At present, there are two intense sources in the few MeV range that allow for low energy neutrino interaction studies. First, the interactions in the

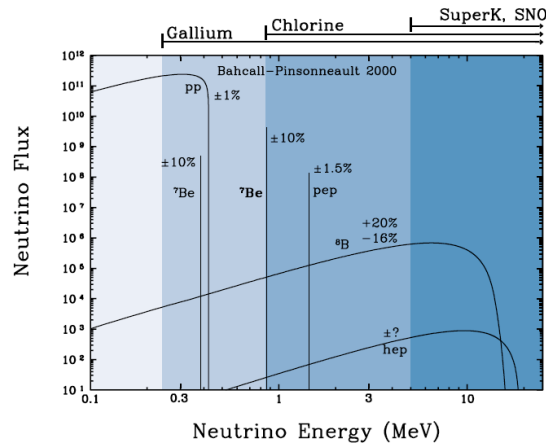


Fig. 5.4. The flux predicted by the Standard Solar Model.¹³ The sensitivity of past solar neutrino detectors varies due to CC threshold in the target material.^{14–16} The thresholds for various experiments is shown at the top of the plot.

Table 5.1. Reactions from the Sun producing neutrinos.

Common Terminology	Reaction
“ <i>pp</i> neutrinos”	$p + p \rightarrow {}^2\text{H} + e^- + \nu_e$
“ <i>pep</i> neutrinos”	$p + e^- + p \rightarrow {}^2\text{H} + \nu_e$
“ ${}^7\text{Be}$ neutrinos”	${}^7\text{Be} + e^- \rightarrow {}^7\text{Li} + \nu_e$
“ ${}^8\text{B}$ neutrinos”	${}^8\text{B} \rightarrow {}^8\text{Be}^* + e^+ + \nu_e$
“ <i>hep</i> neutrinos”	${}^3\text{He} + p \rightarrow {}^4\text{He} + e^+ + \nu_e$

Sun produce a pure ν_e flux, as listed in tab. 5.1. The energy distribution of neutrinos produced by these reactions is shown in Fig. 5.4. The sensitivity of various solar neutrino experiments, due to the CC threshold, is shown at the top of the figure. There is no observable antineutrino content. The best limit on the solar neutrino $\bar{\nu}_e/\nu_e$ ratio for $E_\nu > 8.3$ MeV is 2.8×10^{-4} at 90% CL.¹⁷ The second source is from reactors. In contrast to the Sun, reactors produce a nearly pure $\bar{\nu}_e$ flux. The energy peaks from ~ 3 to 7 MeV. Neutrinos from β decay of accelerated isotopes could, in principle, represent

Table 5.2. Common sources of neutrinos in atmospheric and accelerator experiments.

2-body pion decay	$\pi^+ \rightarrow \mu^+ \nu_\mu, \pi^- \rightarrow \mu^- \bar{\nu}_\mu$
2-body kaon decay	$K^+ \rightarrow \mu^+ \nu_\mu, K^- \rightarrow \mu^- \bar{\nu}_\mu$
muon decay	$\mu^+ \rightarrow e^+ \bar{\nu}_\mu \nu_e, \mu^- \rightarrow e^- \nu_\mu \bar{\nu}_e$
K_{e3} decay	$K^+ \rightarrow \pi^0 e^+ \nu_e, K^- \rightarrow \pi^0 e^- \bar{\nu}_e, K^0 \rightarrow \pi^- e^+ \nu_e, K^0 \rightarrow \pi^+ e^- \bar{\nu}_e$

a third intense source of neutrinos in the MeV range (or higher), once the technical issues involved in designing such an accelerator are overcome. Such a “beta beam” would produce a very pure ν_e or $\bar{\nu}_e$ beam, depending on the accelerated isotope.¹⁸

At present, higher energy experiments use neutrinos produced at accelerators and in the atmosphere. In both cases, neutrinos are dominantly produced via meson decays. In the atmospheric case, cosmic rays hit atmospheric nuclei producing a shower of mesons which may decay to neutrinos along their path through the atmosphere to Earth. In a conventional neutrino beam, protons impinge on a target, usually beryllium or carbon, producing secondary mesons. In many experiments, the charged mesons are focussed (bent) toward the direction of the experiment with a magnetic device called a horn. These devices are sign-selecting – they will focus one charge-sign and defocus the other – and so produce beams which are dominantly neutrinos or antineutrinos depending on the sign-selection. The beamline will have a long secondary meson decay region, which may be air or vacuum. This is followed by a beam dump and an extended region of dirt or shielding to remove all particles except neutrinos. There are excellent reviews of methods of making accelerator-produced neutrino beams.¹⁹ Tab. 5.2 summarizes the common sources of neutrino production in the atmosphere and conventional accelerator based beams.

Many atmospheric and accelerator-based neutrino experiments are designed to study 100 MeV to 10 GeV neutrinos. The atmospheric neutrino flux drops as a power-law with energy, and the 1 to 10 GeV range dominates the event rate. Accelerator beams can be tuned to a specific energy range and, using present facilities, can extend to as high as 500 GeV. From the viewpoint of sheer statistics, one should use the highest energy neutrino beam which is practical for the physics to be addressed, since the cross section rises linearly with energy. However, lower neutrino energy beams, from ~ 1 to 10 GeV, are typically used for oscillation experiments. In these experiments, having a cleanly identified lepton in a low multiplicity event trumps sheer rate, and so ~ 1 GeV beams are selected to assure that CCQE and single pion events dominate the interactions.

Both atmospheric and accelerator based neutrino sources are dominantly ν_μ -flavor. The main source of these neutrinos is pion decay. To understand why pions preferentially decay to produce ν_μ rather than ν_e , consider the case of pion decay to a lepton and an antineutrino: $\pi^- \rightarrow \ell^- \bar{\nu}_\ell$. The pion has spin zero and so the spins of the outgoing leptons from the decay must be opposite from angular momentum conservation. In the center of mass of the pion, this implies that both the antineutrino and the charged lepton have spin projected along the direction of motion (“right” or “positive” helicity). However, this is a weak decay, where the W only couples to the RH antineutrino and the LH component of the charged particle. The amplitude for the LH component to have right-helicity is proportional to m/E . Thus it is very small for an electron compared to the muon, producing a significant suppression for decays to electrons. Calculating the expected branching ratios:

$$R_{theory} = \frac{\Gamma(\pi^\pm \rightarrow e^\pm \nu_e)}{\Gamma(\pi^\pm \rightarrow \mu^\pm \nu_\mu)} \quad (5.7)$$

$$= \left(\frac{m_e}{m_\mu}\right)^2 \left(\frac{m_\pi^2 - m_e^2}{m_\pi^2 - m_\mu^2}\right)^2 \quad (5.8)$$

$$= 1.23 \times 10^{-4}; \quad (5.9)$$

This compares well to the data:²⁰ $R_{exp} = (1.230 \pm 0.004) \times 10^{-4}$.

The above discussion assumed the neutrino was massless. If the neutrino is massive, then it too can be produced with wrong helicity with an amplitude proportional to m_ν/E and thus a probability proportional to $(m_\nu/E)^2$. As discussed in sec. 5.2.2, below, neutrino mass is limited to be very small (\sim eV) and thus the rate of wrong-helicity neutrino production is too low a level for any chance of observation in the near future.

Depending on the energy, there may also be significant neutrino production from kaon decays. The charged kaon preferentially decays to the ν_μ for the same reason as the charged pion. However, for equal energy mesons, the kinematic limit for a neutrino from K^+ decay is much higher than for π^+ decay: $E_\nu^{max,K} = 0.98E_K$ compared to $E_\nu^{max,\pi} = 0.43E_\pi$. Thus the neutrinos from kaon decays can be isolated by studying the highest energy component of a beam. Fig. 5.5 shows the contributions of pion and kaon decays to the ν_μ flux in the MiniBooNE experiment, which uses an 8 GeV primary proton beam.

Electron neutrino flavors are produced in these beams through $K \rightarrow \pi \nu_e e$ (called “Ke3”) decay and through the decay of the muons which were produced in the pion decay. These are three-body decays which avoid substantial helicity suppression. Helicity does, however, affect the energy

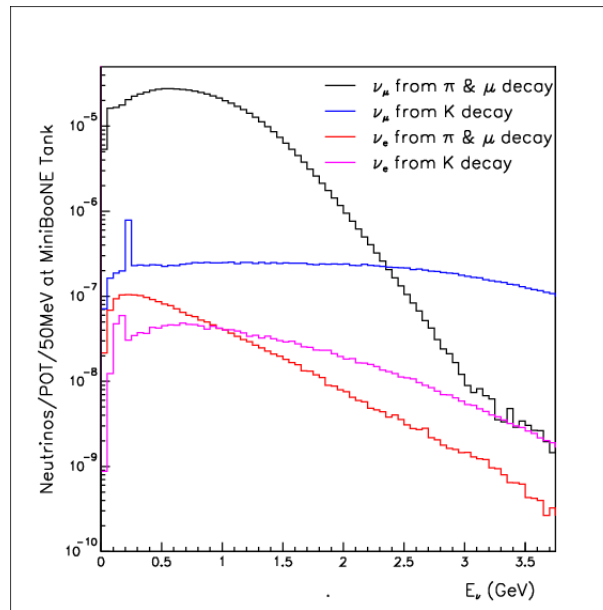


Fig. 5.5. The contributions from pion and kaon production to the total predicted ν_μ flux in the MiniBooNE experiment. The spikes at low energy in the K-produced fluxes are due to decays of stopped kaons in the beam dump.¹⁰

spectrum of the outgoing decay products. In an accelerator-based experiment, the level of electron-flavor content can be regulated, at some level, by the choice of primary beam energy and the length of the decay region. A low primary beam energy will suppress kaon production because of the relatively high mass of this meson (494 MeV). A short decay pipe will suppress ν_e from μ decay, which tends to occur downstream, because it is produced in a multi-step decay chain ($\pi \rightarrow \mu \rightarrow \nu_e$). Both of these methods of suppressing ν_e production also lead to a reduction in the ν_μ production rate, so an experimenter must balance competing goals in the beam design. In the case of atmospheric neutrinos, the ratio is roughly 2:1 for $\nu_\mu:\nu_e$, though

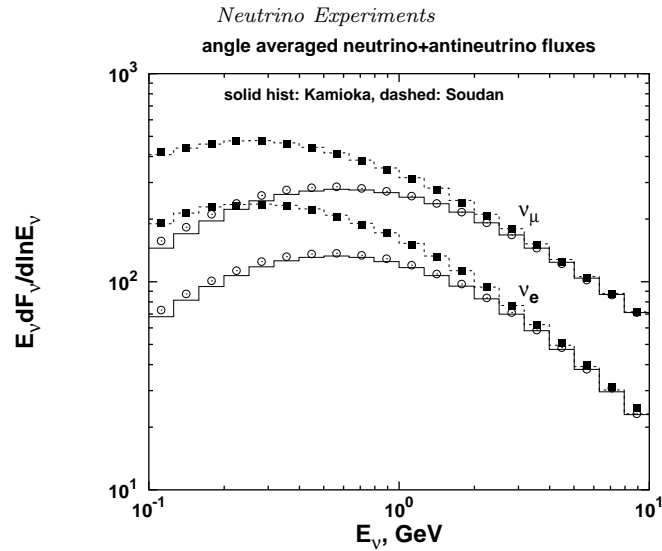


Fig. 5.6. The variation in the atmospheric neutrino flavor content as a function of energy for two locations, Japan (solid line, open circles) and Minnesota (dashed line, closed squares). The points are from a full 3-dimensional monte carlo of the flux, while the histograms are from a simpler model.²¹

the fraction ν_e 's changes with energy (see Fig. 5.6). The atmospheric flux depends on the location of the detector because charged particle are bent by the Earth's magnetic field. The variation between fluxes at the Kamioka mine in Japan and Soudan mine in Minnesota are shown in Fig. 5.6.

As we move to a precision era in neutrino physics, precise "first-principles" predictions of the flux are becoming very important. For conventional accelerator-based neutrino beams and for the atmospheric flux, this requires well-measured cross-sections for production of secondary pions and kaons. This has motivated a range of secondary production experiments. The kinematic coverage is shown on Fig. 5.7.

The future of high intensity ν_μ and ν_e beams is likely to lie in beams produced from muon decay. Because of the potential for very high intensity, these beams are called "Neutrino Factories." The concept is very attractive because it produces beams which are very pure ν_μ and $\bar{\nu}_e$ from μ^- and vice versa from μ^+ . Each flavor has no "wrong sign" (antineutrino-in-neutrino-beam or neutrino-in-antineutrino beam) background. However, neutrino factory designs¹⁸ necessarily produce high energy neutrinos, since the muons must be accelerated to high energies in order to live long enough

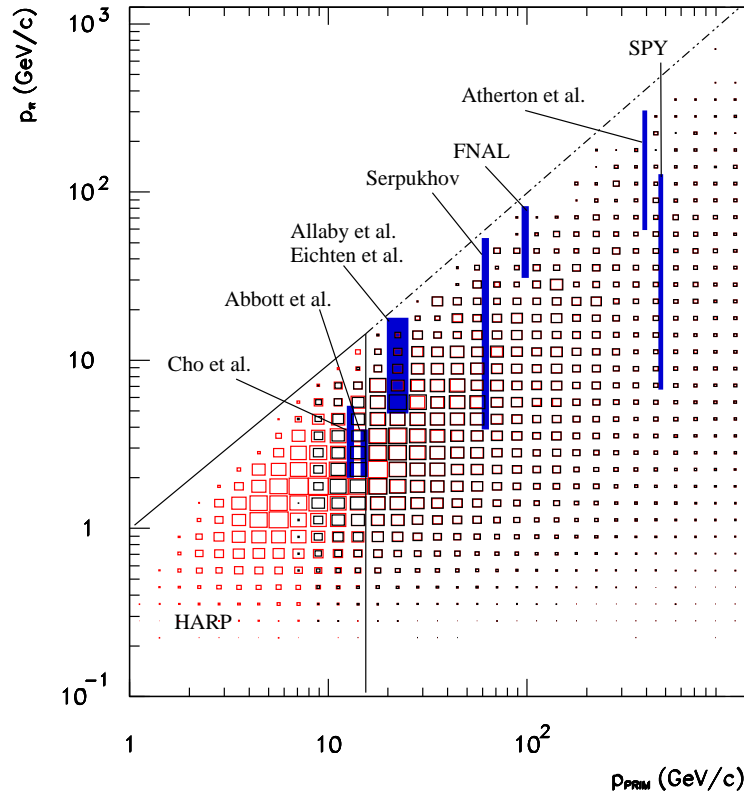


Fig. 5.7. The kinematic range covered by recent experiments measuring secondary pion and kaon production.²⁴

to be captured and circulated in an accelerator. The Neutrino Factory is seen as a promising first machine for testing ideas for a muon collider,¹⁸ and thus has attracted interest beyond the neutrino community.

A beam enriched in ν_τ can be produced by impinging very high energy protons on a target to produce D_s -mesons which are sufficiently massive to decay to $\tau \nu_\tau$. The τ lepton is very massive, at 1.8 GeV, compared to the muon, at 106 MeV, and thus helicity considerations for the D_s decay strongly favor the $\tau \nu_\tau$ mode compared to $\mu \nu_\mu$, by a ratio of about 10:1. The τ then subsequently decays, also producing ν_τ s.

Unfortunately, because of the short lifetime, it is not possible to separate D_s mesons from the other mesons prolifically produced by the primary interaction. As a result, the beam is dominated by the ν_μ s produced by

decays of other mesons. To reduce the production of ν_μ , experiments use a “beam dump” design where protons hit a very thick target where pions can be absorbed before decaying. The only enriched- ν_τ beam created to date was developed by DoNuT.⁶ They used an 800 GeV proton on a beam dump, to produce a ratio of $\nu_e:\nu_\mu:\nu_\tau$ of about 6:9:1.

5.1.4. Typical Neutrino Detectors

Because neutrinos interact so weakly, the options for detectors are limited to designs which can be constructed on a massive scale. There are several general styles in use today: unsegmented scintillator detectors, unsegmented Cerenkov detectors, segmented scintillator-and-iron calorimeters, and segmented scintillator trackers. The most promising future technology is the noble-element based detector, which is effectively an electronic bubble chamber. Liquid argon detectors are likely to be the first large-scale working example of such technology. There are a few variations on these five themes, which are considered in later sections in the context of the measurement.

Unsegmented scintillator detectors are typically used for low energy antineutrino experiments. Recent examples include Chooz,²⁵ KamLAND²⁶ and LSND.²⁷ These consist of large tanks of liquid scintillator surrounded by phototubes. Usually the scintillator is oil based, hence the target material is CH_2 and its associated electrons. Often the tubes are in an pure oil buffer. This reduce backgrounds from radiation emitted from the glass which would excite scintillator. The free protons in the oil provide a target for the interaction, $\bar{\nu}_e p \rightarrow e^+ n$, which is the key for reactor experiments. The reaction threshold for this interaction is 1.806 MeV due to the mass differences between the proton and neutron and the mass of the positron. The scintillation light from the e^+ , as well as light from the Compton scattering of the 0.511 MeV annihilation photons provide an initial (“prompt”) signal. This is followed by n capture to produce deuterium and a 2.2 MeV. This sequence – positron followed by neutron capture – provides a clean signal for the interaction. Doping the liquid scintillator with gadolinium substantially increases the neutron capture cross section as well as the visible energy produced in the form of gammas upon neutron capture.

Unsegmented scintillator detectors are now being introduced for low energy solar neutrino measurements at Borexino,²⁸ KamLAND²⁹ and SNO+.³⁰ These provide energy information on an event-by-event basis, unlike most past solar neutrino experiments, such as Homestake,¹⁴ SAGE¹⁵

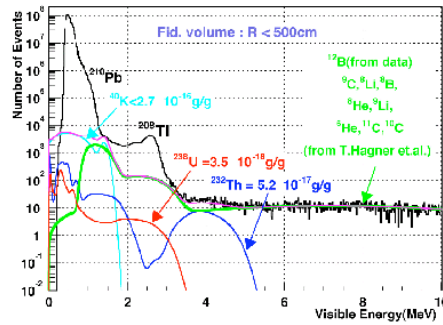


Fig. 5.8. Energy distribution and sources of singles events in KamLAND as a function of visible energy.³¹

and GallEx,¹⁶ which integrated over time and energy. However, these are very difficult experiments to perform because a neutron is not produced and so the scattering does not produce a two-fold coincidence, but only a prompt flash of light.

Environmental backgrounds are by far the most important issue in low energy experiments. These fall into two categories: naturally occurring radioactivity and muon-induced backgrounds. To get a sense for what is expected, Fig. 5.8 shows the visible energy distribution of singles events from the KamLAND experiment with the sources of environmental background identified. The naturally occurring radioactive contaminants mainly populate the low energy range of Fig. 5.8, with isotopes from the U and Th chain extending to the highest energies. These isotopes must be kept under control by maintaining very high standards of cleanliness. The second source of environmental background, the β -decays of isotopes produced by cosmic ray muons. These dominate the background for $E_{\text{visible}} > 4$ MeV (see Fig. 5.8). These can only be eliminated by shielding the detector from cosmic rays. As a result, we must build deep underground laboratories with many thousands of meters-water-equivalent (“mwe”) of rock shielding.

In these scintillator detectors, the CC interaction with the carbon in the oil (which produces either nitrogen or boron depending on whether the scatterer is a neutrino or antineutrino) has a significantly higher energy

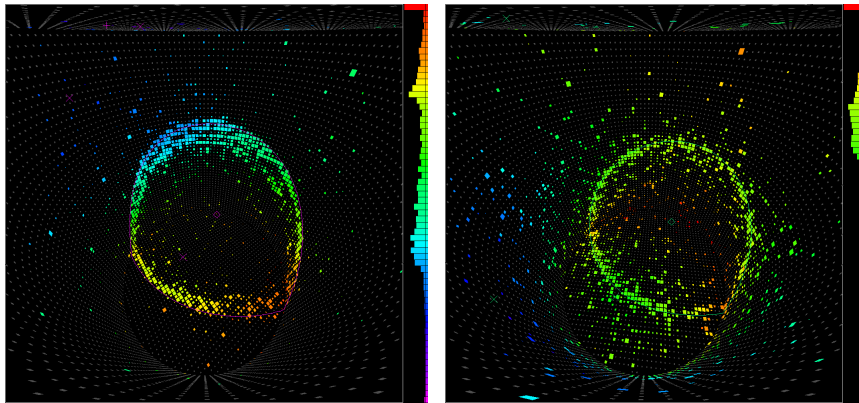


Fig. 5.9. An example of a muon ring (left) and electron ring (right) in the Super K Cerenkov detector.³³

threshold than scattering from free protons. $\nu_e + C \rightarrow e^- + N$ has a threshold energy of 13.369 MeV, which arises from the carbon-nitrogen mass difference (plus the mass of the electron). In the case of both reactor and solar neutrinos, the flux cuts off below this energy threshold.

Existing unsegmented Cerenkov detectors include MiniBooNE,³² Super K,³³ and AMANDA.³⁴ These detectors make use of a target which is a large volume of a clear medium (undoped oil, water and ice, respectively) surrounded by or interspersed with phototubes. Undoped oil has the advantages of a larger refractive index, leading to larger Cerenkov opening angle, and of not requiring a purification system to remove living organisms. Water is the only affordable medium once a detector is larger than a few ktons. For ultra-high energy neutrino experiments, a vast natural target is needed. Sea water³⁵ and ice³⁴ have been used. Ice is, to date, more successful because it does not suffer from backgrounds from bioluminescence.

In most cases of these detectors, the tubes surround the medium and the projected image of the Cerenkov ring is used for particle identification. To understand how this works, first consider the case of a perfect, short track. This will project a ring with a sharp inner and outer edge onto the phototubes. Next consider an electron produced in a ν_e CC quasielastic interaction. Because the electron is low mass, it will multiple scatter and easily bremsstrahlung, smearing the light projected on the tubes and producing a “fuzzy” ring. A muon produced by a CC quasielastic ν_μ interaction is heavier and thus will produce a sharper outer edge to the ring.

For the same visible energy, the track will also extend farther, filling the interior of the ring, and perhaps exit the tank. Fig. 5.9 compares an electron and muon ring observed in the Super K detector. If the muon stops within the tank and subsequently decays, the resulting “michel electron” provides an added tag for particle identification. In the case of the μ^- , 18% will capture in water, and thus have no michel electron tag, while only 8% will capture in oil.

Scintillator and iron calorimeters provide affordable detection for ν_μ interactions in the range of ~ 1 GeV and higher. Recent examples include the MINOS³⁶ and NuTeV³⁷ experiments. In these detectors, the iron provides the target, while the scintillator provides information on energy deposition per unit length. This allows separation between the hadronic shower, which occurs in both NC and CC events, and the minimum ionizing track of an outgoing muon, which occurs in CC events. Transverse information can be obtained if segmented scintillator strips are used, or if drift chambers are interspersed. The light from scintillator strips is transported to tubes by mirrored wave-length-shifting fibers. Transverse information improves separation of electromagnetic and hadronic showers. The iron can be magnetized to allow separation of neutrino and antineutrino events based on the charge of the outgoing lepton.

In all three of the above detector designs, it is difficult to reconstruct multi-particle events. Tracking is not an option for an unsegmented scintillator detector. Cerenkov detectors can typically resolve two tracks per event. Segmented calorimeters reduce multiple hadrons to a shower, obscuring any track-by-track information other than from muons.

To address the problem of track reconstruction in low energy ($\lesssim 1$ GeV), low multiplicity events, there has been a move toward all-scintillator tracking detectors. This began with the SciBar detector in K2K.³⁸ This detector used scintillator strips, as in MINOS, but without interspersing iron. As a result, low energy (few MeV) tracks were clearly observable and quasielastic and single pion events could be fully reconstructed. SciBar has since been incorporated into the SciBooNE experiment at Fermilab.¹¹ The CCQE event in SciBooNE, shown in Fig. 5.10, makes clear the benefits of fine segmentation. The position of the vertex and the short track from the proton are well-resolved in the SciBar detector (green region). The technology has been taken further by the MINERvA experiment, which has attained 2 mm resolution with their prototype.³⁹ SciBar and MINERvA are relatively small (few ton) detectors. The first very large scale application of this technology will be NOvA, which is a future 15 kton detector.⁴⁰ This detector

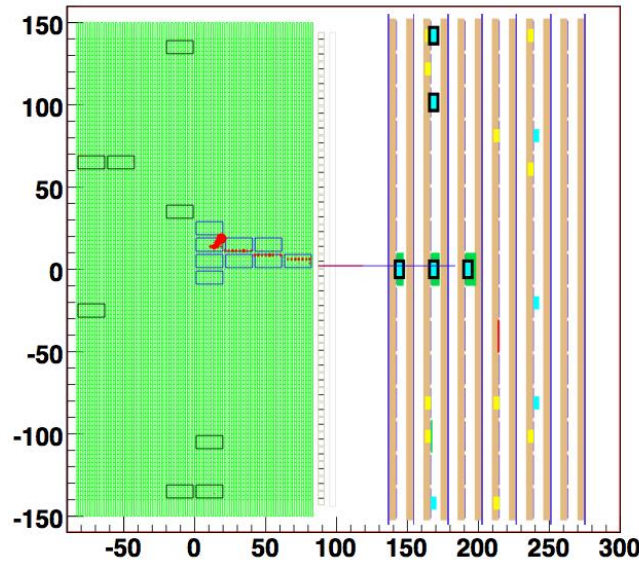


Fig. 5.10. A CCQE($\nu_\mu + n \rightarrow \mu + p$) event observed in the SciBooNE detector. The long, minimum-ionizing red track is identified as the muon, the short, heavily-ionizing red track is identified as the proton.¹¹

will use PVC tubes filled with liquid scintillator, which is more cost-effective than extruded scintillator strips for very large detectors. Their design also loops the wave-length shifting fiber, so that there are, effectively, two perfectly mirrored fibers in each cell. This elegant solution increases the collected light by a factor of four, which is necessary for ~ 15 m strips.

The most promising new technology for high resolution track reconstruction in neutrino physics is the liquid argon TPC. A TPC, or time projection chamber, uses drift chambers to track in the x and y views and drift time to determine the z view. Liquid argon (LAr), which provides the massive target for the neutrino interaction, also scintillates, providing the start for the drift-time measurement. A key point for future neutrino experiments is the high efficiency for identifying electron showers (expected to be 80-90%) with a rejection factor of 70 for NC π^0 events. In particular, these detectors can differentiate between converted photons and electrons through the dE/dx in the first few centimeters of the track. Typical energy resolution for an electromagnetic shower is $3\%/\sqrt{E}$.

There is a great deal of activity on development of LAr detectors. Data

have been taken successfully on a 50 liter LArTPC prototype in the NOMAD neutrino beam at CERN, resulting in reconstruction of ~ 100 CC quasielastic events.⁴¹ Also, recently, a 600 ton Icarus module has been commissioned at Gran Sasso.⁴² A 0.8 ton LAr test detector will begin taking data at Fermilab in January, 2008.⁴³ As discussed in sec. 5.3.2, the microBooNE experiment is a proposed 100 ton detector which would take data in 2010.⁴⁴ In principle, these detectors can be scaled up to tens of ktons, as is discussed in the “Ash River Proposal”.⁴⁵

5.2. Neutrinos As We Know Them Now

The recent discovery of neutrino oscillations requires that we reconsider the Standard Model Lagrangian of sec. 5.1.1. It must now incorporate, preferably in a motivated fashion, both neutrino mass and neutrino mixing. This represents both a challenge and an opportunity for the theory, which I will discuss in the following section. This section concentrates on the experimental discovery. It is interesting to note that while neither neutrino mass nor mixing were “needed” in the Standard Model theory, both are required for the discovery of neutrino oscillations. The probability for neutrino oscillations will be zero unless *both* effects are present.

The outcome of the observation of neutrino oscillations is typically summarized by the statement that “neutrinos have mass.” To be clear: we still have no direct measurement of neutrino mass. At this point, we have clear evidence of mass differences between neutrinos from the observation of neutrino oscillations. A mass difference between two neutrinos necessarily implies that at least one of the neutrinos has non-zero mass. All experimental evidence indicates that the actual values of the neutrino masses are tiny in comparison to the masses of the charged fermions. At the end of this section, attempts at direct measurement of neutrino mass are described.

5.2.1. *Neutrino Oscillations*

Recent results on neutrino oscillations provide indisputable evidence that there is a spectrum of masses for neutrinos. In this section, I describe the formalism for neutrino oscillations, and then review the experimental results which have now been confirmed at the 5σ level. This is covered briefly because these results are well known and covered extensively elsewhere.²

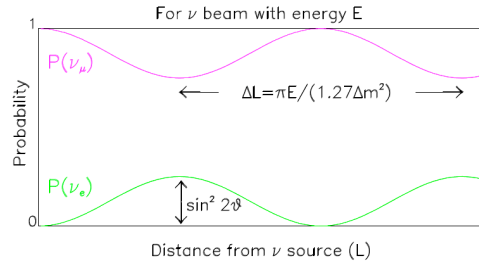


Fig. 5.11. Example of neutrino oscillations as a function of distance from the source, L . The wavelength depends upon the experimental parameters L and E (neutrino energy) and the fundamental parameter Δm^2 . The amplitude of the oscillation is constrained by the mixing term, $\sin^2 2\theta$.

5.2.1.1. The Basic Formalism

Neutrino oscillations requires that neutrinos have mass, that the difference between the masses be small, and that the mass eigenstates be different from the weak interaction eigenstates. In this case, the weak eigenstates can be written as mixtures of the mass eigenstates. For example, in a simple 2-neutrino model:

$$\begin{aligned}\nu_e &= \cos \theta \nu_1 + \sin \theta \nu_2 \\ \nu_\mu &= -\sin \theta \nu_1 + \cos \theta \nu_2\end{aligned}$$

where θ is the “mixing angle.” In this case, a pure flavor (weak) eigenstate born through a weak decay can oscillate into another flavor as the state propagates in space. This oscillation is due to the fact that each of the mass eigenstate components propagates with different frequencies if the masses are different, $\Delta m^2 = |m_2^2 - m_1^2| > 0$. In such a two-component model, the oscillation probability for $\nu_\mu \rightarrow \nu_e$ oscillations is then given by:

$$\text{Prob}(\nu_\mu \rightarrow \nu_e) = \sin^2 2\theta \sin^2 \left(\frac{1.27 \Delta m^2 (\text{eV}^2) L (\text{km})}{E (\text{GeV})} \right), \quad (5.10)$$

where L is the distance from the source, and E is the neutrino energy. As shown in Fig. 5.11, the oscillation wavelength will depend upon L , E , and Δm^2 . The amplitude will depend upon $\sin^2 2\theta$.

Neutrino oscillations only occur if the two mass states involved have sufficiently small Δm^2 that the neutrino flavor is produced in a superposition of two mass states. If the mass splitting is sufficiently large, a given neutrino flavor would be produced in one or the other of the two mass eigenstates and interference (*i.e.*, oscillations) would not occur.

Most neutrino oscillation analyses consider only two-generation mixing scenarios, but the more general case includes oscillations among all three neutrino species. This can be expressed as:

$$\begin{pmatrix} \nu_e \\ \nu_\mu \\ \nu_\tau \end{pmatrix} = \begin{pmatrix} U_{e1} & U_{e2} & U_{e3} \\ U_{\mu 1} & U_{\mu 2} & U_{\mu 3} \\ U_{\tau 1} & U_{\tau 2} & U_{\tau 3} \end{pmatrix} \begin{pmatrix} \nu_1 \\ \nu_2 \\ \nu_3 \end{pmatrix}.$$

This formalism is analogous to the quark sector, where strong and weak eigenstates are not identical and the resultant mixing is described conventionally by a unitary mixing matrix. The oscillation probability is then:

$$\text{Prob}(\nu_\alpha \rightarrow \nu_\beta) = \delta_{\alpha\beta} - 4 \sum_{j>i} U_{\alpha i} U_{\beta i}^* U_{\alpha j}^* U_{\beta j} \sin^2 \left(\frac{1.27 \Delta m_{ij}^2 L}{E} \right), \quad (5.11)$$

where $\Delta m_{ij}^2 = m_j^2 - m_i^2$, α and β are flavor-state indices (e, μ, τ) and i and j are mass-state indices (1, 2, 3).

For three neutrino mass states, there are three different Δm^2 parameters, although only two are independent since the two small Δm^2 parameters must sum to the largest. The neutrino mass states, ν_1 , ν_2 and ν_3 are defined such that the difference between ν_1 and ν_2 always represents the smallest splitting. However, the mass of ν_3 relative to ν_1 and ν_2 is arbitrary and so the sign of the Δm^2 parameters which include the third mass state may be positive or negative. That is, if $\nu_3 > \nu_1, \nu_2$, then Δm_{23}^2 will be positive, but if $\nu_1, \nu_2 > \nu_3$, then Δm_{23}^2 will be negative. The former is called a “normal mass hierarchy” and the latter is the “inverted mass hierarchy.” At this point, the sign is irrelevant because Δm^2 appears in a term which is squared. However, in sec. 5.3.1, this point will become important.

The mixing matrix above can be described in terms of three mixing

angles, θ_{12} , θ_{13} and θ_{23} :

$$U = \begin{pmatrix} c_{12}c_{13} & s_{12}c_{13} & s_{13} \\ -s_{12}c_{23} - c_{12}s_{23}s_{13} & c_{12}c_{23} - s_{12}s_{23}s_{13} & s_{23}c_{13} \\ s_{12}s_{23} - c_{12}c_{23}s_{13} & -c_{12}s_{23} - s_{12}c_{23}s_{13} & c_{23}c_{13} \end{pmatrix}, \quad (5.12)$$

where $c_{ij} \equiv \cos \theta_{ij}$ and $s_{ij} \equiv \sin \theta_{ij}$, with i and j referring to the mass states. In fits to the oscillation parameters, people variously quote the results in terms of the matrix element of U , sin-squared of the given angle, sin-squared of twice the angle and a variety of other forms, all of which are related. Using the 13 case as an example, the quoted parameters are related by:

$$U_{e3}^2 \approx \sin^2 \theta_{13} \approx \frac{1}{4} \sin^2 2\theta_{13}. \quad (5.13)$$

Thus, in total, there are five free parameters in the simplest three-neutrino oscillation model, which can be taken to be Δm_{12}^2 , Δm_{23}^2 , θ_{12} , θ_{13} and θ_{23} .

Although in general there will be mixing among all three flavors of neutrinos, two-generation mixing is often assumed for simplicity. If the mass scales are quite different ($m_3 \gg m_2 \gg m_1$, for example), then the oscillation phenomena tend to decouple and the two-generation mixing model is a good approximation in limited regions. In this case, each transition can be described by a two-generation mixing equation. However, it is possible that experimental results interpreted within the two-generation mixing formalism may indicate very different Δm^2 scales with quite different apparent strengths for the same oscillation. This is because, as is evident from equation 5.11, multiple terms involving different mixing strengths and Δm^2 values contribute to the transition probability for $\nu_\alpha \rightarrow \nu_\beta$.

5.2.1.2. Matter Effects

The probability for neutrino oscillations is modified in the presence of matter. This is true in any material, however the idea was first explored for neutrino oscillations in the Sun, by Mikheyev, Smirnov and Wolfenstein. Therefore, matter effects are often called “MSW” effects.⁴⁶ In general, matter effects arise in neutrino-electron scattering. The electron neutrino flavor experiences both CC and NC elastic forward-scattering with electrons. However, the ν_μ and ν_τ experience only NC forward-scattering, because creation of the μ or τ is kinematically forbidden or suppressed (e.g. $\nu_\mu + e^- \rightarrow \nu_e + \mu^-$). This difference produces the matter effect.

For neutrinos propagating through a constant density of electrons, if V_e is the elastic forward scattering potential for the ν_e component, and V_{other} is the potential for the other neutrino flavors, then the additional scattering potential is

$$V = V_e - V_{other} = \sqrt{2}G_F n_e, \quad (5.14)$$

where G_F is the Fermi constant and n_e is the electron density. This potential modifies the Hamiltonian, so that, if H_0 is the vacuum Hamiltonian, then in matter the Hamiltonian is $H_0 + V$. This means that the eigenstates are modified from those of a vacuum, ν_1 and ν_2 , to become ν_{1m} and ν_{2m} . Effectively, the neutrino mass spectrum is not the same as in vacuum. The solutions to the Hamiltonian are also modified. From this, one can see that the presence of electrons may substantially change the oscillatory behavior of neutrinos.

The simplest outcome is that matter induces a shift in the mass state, which is a combination of flavor eigenstates, propagates through the material. This leads to a change in the oscillation probability:

$$\text{Prob}(\nu_e \rightarrow \nu_\mu) = (\sin^2 2\theta/W^2) \sin^2 (1.27W\Delta m^2 L/E) \quad (5.15)$$

where $W^2 = \sin^2 2\theta + (\sqrt{2}G_F n_e (2E/\Delta m^2) - \cos 2\theta)^2$ (Note that in a vacuum, where $n_e = 0$, this reduces to equation 5.10.) From this, one can see that if a neutrino, passing through matter, encounters an optimal density of electrons, a “resonance,” or large enhancement of the oscillation probability, can occur. The Sun has a wide range of electron densities and thus is a prime candidate for causing matter effects. Also, neutrinos traveling through the Earth’s core, which has a high electron density, might experience matter effects. This will produce a “day-night effect,” or sidereal variation, for neutrinos from the Sun.

For situations like the Sun, with very high electron densities which vary with the position of the neutrino (and hence the time which the neutrino has lived), the situation is complex. If the electron density is high and the density variation occurs slowly, or adiabatically, then transition (not oscillation!) between flavors in the mass state can occur as the neutrino propagates. Thus it is possible for neutrinos to be produced in the core of the Sun in a given mass and flavor state, and slowly evolve in flavor content until the neutrino exits the Sun, still in the same mass state. In other words, in the Sun, a ν_e produced in a mass eigenstate $\nu_{2m}(r)$, which depends on the local electron density at radius r , propagates as a ν_{2m} until

it reaches the $r = R_{\text{solar}}$, where $\nu_{2m}(R_{\text{solar}}) = \nu_2$. This peculiar effect is called the Large Mixing Angle MSW solution.

5.2.1.3. Designing an Oscillation Experiment

From equation 5.10, one can see that three important issues confront the designer of the ideal neutrino experiment. First, if one is searching for oscillations in the very small Δm^2 region, then large L/E must be chosen in order to enhance the $\sin^2(1.27\Delta m^2 L/E)$ term. However if L/E is too large in comparison to Δm^2 , then oscillations occur rapidly. Because experiments have finite resolution on L and E , and a spread in beam energies, the $\sin^2(1.27\Delta m^2 L/E)$ averages to $1/2$ when $\Delta m^2 \gg L/E$ and one loses sensitivity to Δm^2 . Finally, because the probability is directly proportional to $\sin^2 2\theta$, if the mixing angle is small, then high statistics are required to observe an oscillation signal.

There are two types of oscillation searches: “disappearance” and “appearance.” To be simplistic, consider a pure source of neutrinos of type x . In a disappearance experiment, one looks for a deficit in the expected flux of ν_x . This requires accurate knowledge of the flux, which is often difficult to predict from first principles. Therefore, most modern disappearance experiments employ a near-far detector design. The near detector measures the flux prior to oscillation (the design goal is to effectively locate it at $L = 0$ in Fig. 5.11). This is then used to predict the unoscillated event rate in the far detector. A deficit compared to prediction indicates disappearance. Appearance experiments search for $\nu_\alpha \rightarrow \nu_\beta$ by directly observing interactions of neutrinos of type β . The case for oscillations is most persuasive if the deficit or excess has the (L/E) dependence predicted by the neutrino oscillation formula (equation 5.10).

The “sensitivity” of an experiment is defined as the average expected limit if the experiment were performed many times with no true signal (only background). Let us consider the sensitivity for a hypothetical perfect (no-systematic error) disappearance neutrino oscillation experiment with N events. A typical choice of confidence level is 90%, so in this case, the limiting probability, assuming there is no signal, is

$$P = \sigma\sqrt{N}/N. \quad (5.16)$$

There are two possible choices of σ associated with a 90% CL sensitivity, depending on the underlying philosophy. If one assumes there is no signal in the data, then one quotes the sensitivity based on 90% of a single-sided

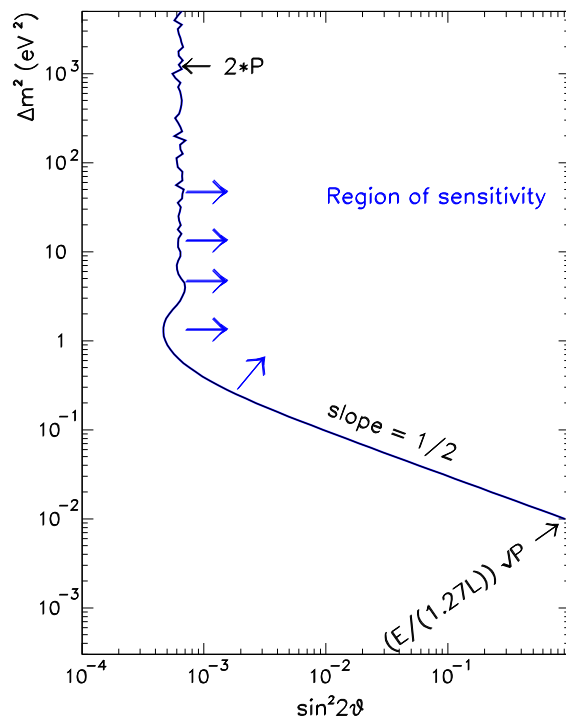


Fig. 5.12. An illustration of the sensitivity of an imaginary oscillation experiment. The region of sensitivity for an experiment depends on the oscillation probability, P , where one can set a limit at some confidence level. Most experiments use 90% CL. The boundaries depend on P , L and E .

Gaussian, which is $\sigma = 1.28$. If the philosophy is that there is a signal which is too small to measure, then one quotes the sensitivity using $\sigma = 1.64$, which is appropriate for a double-sided Gaussian. Historically, $\sigma = 1.28$ was used in most publications. Physicists engage in arguments as to which is most correct, but what is most important from a practical point of view is for the reader to understand what was used. The reader can always scale

between 1.28 and 1.64 depending on personal opinion.

There is only one measurement, P , and there are two unknowns, Δm^2 and $\sin^2 2\theta$; so this translates to a region of sensitivity within $\Delta m^2 - \sin^2 2\theta$ space. This is typically indicated by a solid line, with the allowed region on the right on a plot (see illustration in Fig 5.12). For the perfect (no-systematic error) experiment, the high Δm^2 limit on $\sin^2 2\theta$ is driven by the statistics. On the other hand, the L and E of the experiment drive the low Δm^2 limit, which depends on the fourth root of the statistics. If our perfect experiment had seen a signal, the indications of neutrino oscillations would appear as “allowed regions,” or shaded areas on plots of Δm^2 vs. $\sin^2 2\theta$.

This rule of thumb – that statistics drives the $\sin^2 2\theta$ -reach and L/E drives the Δm^2 reach – becomes more complicated when systematics are considered. The imperfections of a real experiment affect the limits which can be set. Systematic uncertainties in the efficiencies and backgrounds reduce the sensitivity of a given experiment. Background sources introduce multiple flavors of neutrinos in the beam. Misidentification of the interacting neutrino flavor in the detector can mimic oscillation signatures. In addition, systematic uncertainties in the relative acceptance versus distance and energy need to be understood and included in the analysis of the data.

For a real experiment, with both statistical and systematic errors, finding the sensitivity and final limit or allowed region requires a fit to the data. The data are compared to the expectation for oscillation across the range of oscillation parameters, and the set of parameters where the agreement is good to 90% CL are chosen. Historically, there are three main approaches which have been used in fits. The first method is the “single sided raster scan.” In this case one chooses a Δm^2 value and scans through the $\sin^2 2\theta$ -space to find the 90% CL limit. The second method, the “global scan,” explores Δm^2 - and $\sin^2 2\theta$ -space simultaneously. Thus there are two parameters to fit and two degrees of freedom. The third method is the frequentist, or “Feldman-Cousins” approach,⁴⁷ in which one simulates “fake-experiments” for each Δm^2 and $\sin^2 2\theta$ point, and determines the limit where, in 90% of the cases, no signal is observed. Each method has pros and cons and the choice is something of a matter of taste. As with the question of a single- or double-sided gaussian, what is important is to compare sensitivities, limits, and signals from like methods.

It is possible for an experiment which does not observe a signal to set a limit which is better than the sensitivity. This occurs if the experiment observed a downward fluctuation in the background. In this case, a limit is hard to interpret. The latest standard practice is to show the sensitivity

and the limit on plots, and the readers can draw their own interpretation.⁴⁷

5.2.1.4. *Experimental Evidence for Oscillations*

Two separate allowed regions in Δm^2 -and- $\sin^2 2\theta$ -space for neutrino oscillations have been observed at the $> 5\sigma$ level. These are called the “Atmospheric Δm^2 ” and “Solar Δm^2 ” regions. The names are historical, as will be seen below. Many reviews have been written on these results (see, for example,^{2, 48 and 49}) and so here the results are briefly outlined.

The highest Δm^2 signal was first observed using neutrinos produced in the upper atmosphere. These atmospheric neutrinos are produced through collisions of cosmic rays with the atmosphere. The neutrinos are detected through their charged-current interactions in detectors on the Earth’s surface.

The first evidence for atmospheric neutrino oscillations came from the Kamioka⁵⁰ and IMB⁵¹ experiments. This was followed by the convincing case presented by the Super K experiment.⁵³ These were single detector experiments observing atmospheric neutrino interactions as a function of zenith angle (see Fig. 5.13). Several striking features were observed. The first was that the ν_μ flavor neutrinos showed clear evidence of disappearance while the ν_e flavor CC scatters were in good agreement with prediction. The second striking observation was that the apparent mixing was nearly maximal. In other words, the experiments were seeing a 50% reduction of the ν_μ event rate compared to expectation.

Complications in the analysis arise from the difficulty in understanding production of atmospheric neutrinos (affecting the understanding of E) and in the accurate reconstruction of events as a function of zenith angle (affecting knowledge of L). The Δm^2 extracted from the Kamoikande data is an order of magnitude higher than that extracted from the Super K data, indicating a clear systematic effect. Thus, it was absolutely crucial for accelerator-based “long-baseline” neutrino experiments to confirm this result. In these experiments, the L is well defined by the distance from source to detector, and the E is well understood from a near detector measurement.

The challenge for long-baseline experiments is that the L/E required to access the atmospheric signal is on the order of 1000 km/GeV. If the beam is relatively low energy, so that the easy-to-reconstruct CCQE interaction dominates the events, then L is on the order of 1000 km. This leads to two major technical challenges. First, because the Earth is a sphere, if the

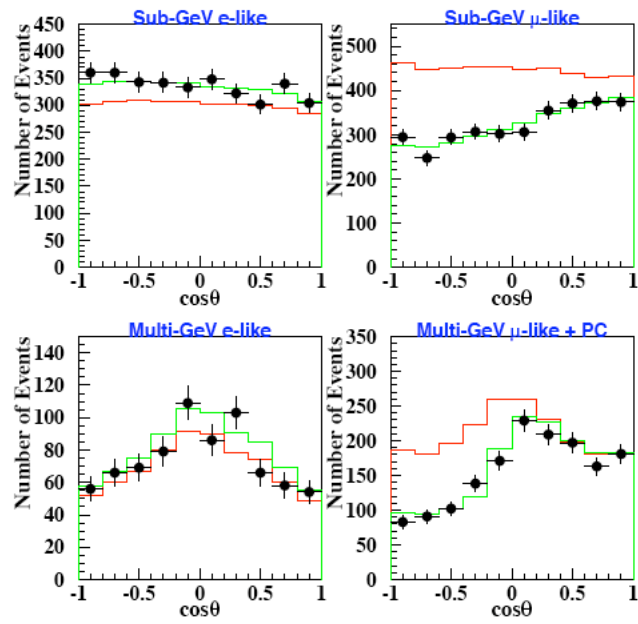


Fig. 5.13. Event rates observed in Super K as a function of zenith angle for two energy ranges. Candidate ν_e events are on the left, ν_μ are on the right. The red line indicates the predicted rate. The green line is the best fit including oscillations.⁵²

source and detector are to be located on (or near) the surface, the beam must be directed downward, into the Earth. Engineering a beamline at a steep angle requires overcoming substantial hurdles in tunneling. Second, the beam spreads as it travels outward from the source, resulting in low intensity at the detector. Therefore, very high rates are needed. However, these challenges have now been overcome at three accelerator complexes: KEK, FNAL and CERN, and a new long-baseline beam from the JPARC facility will be available soon. Making use of these lines, initial confirmation of the atmospheric neutrino deficit came from the KEK-to-Kamiokande (K2K) long baseline experiment.⁵⁴ This has since been followed up by the MINOS experiment to high precision.^{55,56}

In the atmospheric data, the ν_e CC signal is in agreement with expectation, and in the long-baseline experiments, no ν_e excess has been observed. Therefore, one cannot interpret this oscillation signal as $\nu_\mu \rightarrow \nu_e$. This leaves only $\nu_\mu \rightarrow \nu_\tau$ as an explanation for the deficit in a three-neutrino model. Observation of ν_τ CC interactions is experimentally difficult in these experiments for a number of reasons. First, the L/E of the signal is such that for lengths available to present experiments, the energy of the beam must be low ($\lesssim 10$ GeV). As discussed in sec. 5.1.2, because the τ mass is 1.8 GeV, there is substantial mass suppression for τ production at low energies, so the CC event rate is low. Second, the τ decays quickly, leaving behind a complicated event structure which can be easily confused with ν_μ and ν_e low multiplicity interactions in calorimeter or Cerenkov detectors. The difficulty of identifying ν_τ events even in a specialized emulsion-based detector with a high energy neutrino beam, was made clear by the DoNuT experiment,⁶ which provided the first, and so far only, direct observation of CC ν_τ interactions. Thus, while some studies claim observation of ν_τ CC interactions in SuperK,⁵⁷ these results are not very convincing to this author. Fortunately, a specialized experiment called OPERA,⁵⁸ which is an emulsion-based long-baseline detector, is presently taking data. The average energy of the CNGS beam used by this experiment is 17 GeV, sufficiently high to produce ν_τ CC events. This experiment is expected to observe ~ 15 events in 5 years of running if the atmospheric neutrino deficit is due to $\nu_\mu \rightarrow \nu_\tau$ with $\Delta m^2 = 2.5 \times 10^{-3} \text{ eV}^2$.⁵⁹

The lower Δm^2 signal is called the “Solar Neutrino Deficit,” as it was first observed as a low rate of observed ν_e ’s from the Sun. The first observation of this effect was a ν_e deficit observed using a Cl target¹⁴ by Ray Davis and collaborators at Homestake, using $\nu_e + \text{Cl} \rightarrow e + \text{Ar}$. Only about 1/3 of the total expected neutrino event rate was observed. By 1999, four additional experiments had confirmed these observations. The GALLEX¹⁶ and SAGE¹⁵ experiments confirmed a deficit for CC electron neutrino interactions in a Ga target producing Ge. The Super Kamiokande experiment observed a deficit for $\nu_e + e \rightarrow \nu_e + e$ reactions in water.²² The deficit is shown on Fig. 5.14, indicated by the blue points. This plot shows the ratio to the Standard Solar Model prediction, which is indicated by the solid line at unity.

A few aspects of the initial solar neutrino deficit studies should be noted. First, the three types of experiments, chlorine-based, gallium-based, and water-based, measured different levels of deficit. Given that each type of nucleus has a different low energy threshold for observation of CC events,

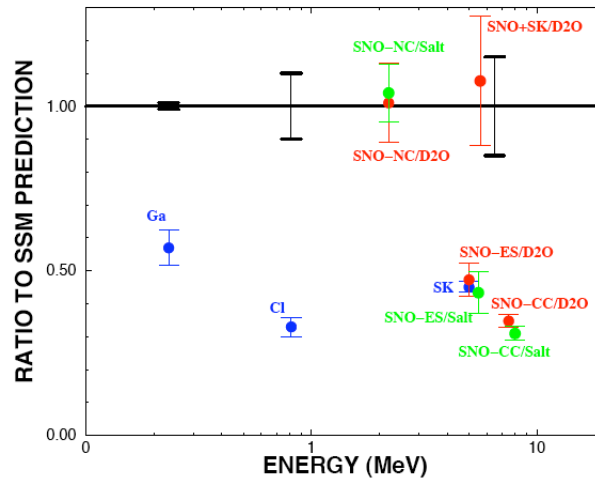


Fig. 5.14. Ratio of observed event rates in solar neutrino experiments compared to the Standard Solar Model. Experiments are plotted at the average energy of the detected signal, which varies due to detection threshold. Black error bars indicate Standard Solar Model error.²³

as previously discussed, one can interpret the varying levels of deficit as an energy dependent effect. Second, all of the above experiments rely upon the CC interaction. The energy of neutrinos from the Sun is so low, that should ν_μ or ν_τ be produced through oscillations, the CC interaction could not occur. This is because of the relatively high mass of the μ (106 MeV) and the τ (1.8 GeV). Thus all of these experiments can observe that ν_e s disappeared, but they cannot observe if the neutrinos reappear as one of the other flavors. This makes a decisive statement that the effect is due to neutrino oscillations problematic.

For some time, people argued the apparent deficit was due to an incomplete picture of solar processes. The two important theoretical issues related to the solar neutrino fluxes were the fusion cross sections and the temperature of the solar interior. A comprehensive analysis of the available information on nuclear fusion cross sections important to solar processes has been compiled⁶⁰ and shows that the important cross sections are well-

known. Results in helioseismology provided an important further test of the “Standard Solar Model”.⁶¹ The Sun is a resonant cavity, with oscillation frequencies dependent upon P/ρ , the ratio of pressure to density. Helioseismological data confirmed the SSM prediction of U to better than 0.1%.⁶² With the results of these studies, most physicists were convinced that the Standard Solar Model was substantially correct. The error bars on the black line at unity in Fig. 5.14 shows the side of the estimated systematic error on the Standard Solar Model.

Interpreting the results as neutrino oscillations resulted in a complicated picture. The vacuum oscillation probability, calculated using equation 5.10, results in allowed regions of Δm^2 which are very low ($\Delta m^2 \sim 10^{-10} \text{eV}^2$). This is because the energy of the neutrinos is only a few MeV, and the Sun to the Earth pathlength is very long ($\sim 10^{11} \text{m}$). On the other hand, the Sun has high electron content and density, so matter effects (sec. 5.2.1.2) could interfere with the picture, allowing higher true values of Δm^2 . The MSW effect yielded two solutions in fits to the data. One was at mixing angles of $\sim 10^{-3}$. Until very recently, this was regarded as the most likely solution based on analogy with mixing in the quark sector. The other solution gave a very large, although not maximal, mixing angle.

Two dramatic results of the early 2000’s demonstrated that the solar neutrino deficit was due to oscillations with the MSW effect and with large mixing angle. The first result was from the SNO experiment.⁶³ SNO used a D_2O target which allowed for measurement of both CC ν_e interactions as well as $\nu + d \rightarrow \nu + n + p$. In the former measurement, SNO sees a deficit consistent with the other measurements within an oscillation interpretation, and which yields a ν_e flux of $(1.76 \pm 0.05(\text{stat}) \pm 0.09(\text{sys})) \times 10^6/\text{cm}^2\text{s}$.⁶⁴ The later measurement is an NC interaction, and thus is flavor-blind. It yields a total NC flux of $(5.09^{+0.44}_{-0.43}(\text{stat})^{+0.46}_{-0.43}(\text{sys})) \times 10^6/\text{cm}^2\text{s}$ ⁶⁴ which can be compared with the theoretical prediction of $(5.69 \pm 0.91) \times 10^6/\text{cm}^2\text{s}$.⁶⁵ In other words, SNO observed the expected total event rate, within errors. This implied that the ν_e s are oscillating to neutrinos which participate in the NC interaction, ν_μ s and/or ν_τ s, with the total $\nu_\mu + \nu_\tau$ flux equal to $(3.41 \pm 0.45(\text{stat})^{+0.48}_{-0.45}(\text{sys})) \times 10^6/\text{cm}^2\text{s}$.⁶⁴ The results of two runs of the SNO experiment are shown by the red and green points on Fig. 5.14. The second result was from the KamLAND experiment. This was a reactor-based experiment located in Japan. Using many reactors which were hundreds of kilometers away, the KamLAND experiment was able to reach $L/E \sim 10^{-6} \text{m/MeV}$. This covered the MSW allowed- Δm^2 solution. The statistics were on the order of hundreds of events, but this was enough

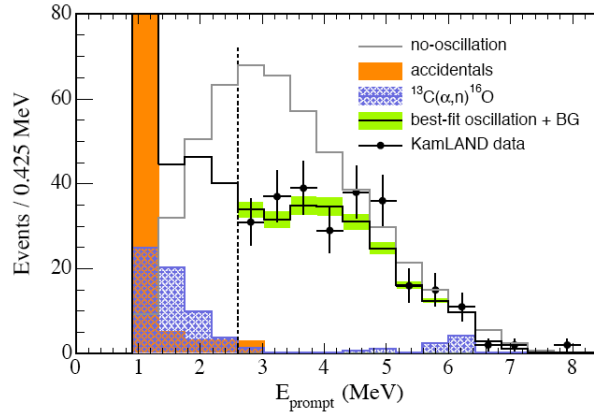


Fig. 5.15. Events in KamLAND as a function of energy. The grey line indicates the expectation for no oscillation.⁶⁶

to probe the large mixing-angle MSW solution. KamLAND expected 365 events and observed 258 events, and thus had clear evidence for oscillations with large mixing, $\tan^2 \theta = 0.40^{+0.010}_{-0.07}$ and relatively high Δm^2 , of $7.9^{+0.6}_{-0.5} \times 10^{-5} \text{ eV}^2$.⁶⁶ The energy distribution of the events observed in KamLAND is shown in Fig. 5.15.

Based on the atmospheric and solar studies, there are two squared mass differences: $\Delta m_{\text{solar}}^2$ and $\Delta m_{\text{atmos}}^2$. The smaller is identified with the mass splitting between ν_1 and ν_2 : $\Delta m_{12}^2 = \Delta m_{\text{solar}}^2$. The atmospheric deficit measures a combination of Δm_{23}^2 and Δm_{13}^2 . However, since $\Delta m_{13}^2 = \Delta m_{12}^2 + \Delta m_{23}^2$ and Δm_{12}^2 is small, $\Delta m_{13}^2 \approx \Delta m_{23}^2 \approx \Delta m_{\text{atmos}}^2$.

A recent global analysis of the data⁶⁷ from the above experiments yields a consistent picture for three neutrino oscillations with five free parameters. The mass differences are: $\Delta m_{12}^2 = (7.9 \pm 0.3) \times 10^{-5} \text{ eV}^2$ and $|\Delta m_{13}^2| = (2.5^{+0.20}_{-0.25}) \times 10^{-5} \text{ eV}^2$, where the absolute value is indicated in the second case because the sign (*i.e.* the mass hierarchy) is unknown. The two well-measured mixing angles are determined to be: $\sin^2 \theta_{12} = 0.30^{+0.02}_{-0.03}$ and

Table 5.3. Selected predictions for $\sin^2 2\theta_{13}$.¹⁰⁴

Model(s)	Refs.	approximate $\sin^2 2\theta_{13}$
Minimal SO(10)	68	0.13
Orbifold SO(10)	69	0.04
SO(10) + Flavor symmetry	70	$1.2 \cdot 10^{-6}$
	71	$7.8 \cdot 10^{-4}$
	72–74	0.01 .. 0.04
	75–77	0.09 .. 0.18
	78	$4 \cdot 10^{-4}$.. 0.01
SO(10) + Texture	79	0.04
	80	0.09
SU(2) _L × SU(2) _R × SU(4) _c		
Flavor symmetries	81–83	0
	84,85,94	$\lesssim 0.004$
	87–89	10^{-4} .. 0.02
	90–94	0.04 .. 0.15
Textures	95	$4 \cdot 10^{-4}$.. 0.01
	96–99	0.03 .. 0.15
3 × 2 see-saw	100	0.04
Anarchy	101	> 0.04
Renormalization group enhancement	102	0.03 .. 0.04
M-Theory model	103	10^{-4}

$\sin^2 \theta_{23} = 0.50^{+0.08}_{-0.07}$. One mixing angle, θ_{13} is yet to be measured, but a limit of $\sin^2 \theta_{13} < 0.025$ can be placed based on global fits.

Based on the measurements, the mixing matrix of eq. 5.12, translates roughly into:

$$U = \begin{pmatrix} 0.8 & 0.5 & ? \\ 0.4 & 0.6 & 0.7 \\ 0.4 & 0.6 & 0.7 \end{pmatrix}. \quad (5.17)$$

This matrix, with its large off-diagonal components, looks very different from the quark-sector mixing matrix where the off-diagonal elements are all relatively small. In this matrix, the “odd element out” is U_{e3} which is clearly substantially smaller than the others. At this point, there is no consensus on what this matrix may be telling us about the larger theory, but there is a sense that the value of θ_{13} is an important clue. Theories which attempt to explain this matrix tend to fall into two classes – those where θ_{13} is just below the present limit and those with very small values. As an illustration of this point, Tab. 5.3 shows order of magnitude predictions for a variety of theories. Thus a measurement of $\sin^2 2\theta_{13}$ which is greater than about 1%, or a limit at this level, can point the way to the larger theory.

The best method for measuring θ_{13} is from reactor experiments which constrain this oscillation by searching for $\bar{\nu}_e$ disappearance. The oscillation

probability is given by:

$$P_{\text{reactor}} \simeq \sin^2 2\theta_{13} \sin^2 \Delta + \alpha^2 \Delta^2 \cos^4 \theta_{13} \sin^2 2\theta_{12}, \quad (5.18)$$

with

$$\alpha \equiv \Delta m_{21}^2 / \Delta m_{23}^2 \quad (5.19)$$

$$\Delta \equiv \Delta m_{31}^2 L / (4E_\nu). \quad (5.20)$$

Events are detected through the inverse beta decay (IBD) interaction. The CHOOZ experiment,²⁵ with a baseline of 1.1 km and typical neutrino event energies between 3 and 5 MeV ($\langle E \rangle = 3.5$ MeV) has set the best reactor-based limit to date, of $\sin^2 2\theta_{13} < 0.27$ at $\Delta m^2 = 2.5 \times 10^{-3} \text{ eV}^2$. This limit can be improved with a global fit, as quoted above.

Significant improvement is expected from the upcoming round of reactor experiments results due to introducing a near-far detector design. The near detector measures the unoscillated event rate, and the far detector is used to search for a deficit as a function of energy. The Double Chooz experiment, beginning in 2009, is expected to reach $\sin^2 2\theta_{13} \sim 0.03$.¹⁰⁵ This will be followed by the Daya Bay experiment which will reach ~ 0.01 .¹⁰⁶

5.2.2. Direct Measurements of Neutrino Mass

For neutrinos, there are no mass measurements, only mass limits. Observations of neutrino oscillations are sensitive to the mass differences between neutrinos, not the actual mass of the neutrino. Therefore, they do not fall into the category of a “direct measurement”. One can, however, use these oscillation results to estimate the required sensitivity for a direct mass measurement. The upper limit comes from assuming that one of the neutrino masses is exactly zero. Given that the largest Δm^2 is $\sim 3 \times 10^{-3} \text{ eV}^2$, this implies there is a neutrino with mass $\sqrt{\Delta m^2} \sim 0.05 \text{ eV}$. The mass of the neutrino can be directly measured from decay kinematics and from time of flight from supernovae. Neither method has reached the 0.05 eV range yet, although the next generation of decay-based experiments comes close.

We know from neutrino oscillations that there is a very poor correspondence between neutrino flavors and neutrino masses, *i.e.*, the mixings are large. However, it is easiest to conduct the discussion of these limits in terms of specific flavors. Thus, what is actually being studied is an average mass associated with each flavor. For example, for the ν_e mass measured from β decay, which will be expanded upon below, what is actually probed

Table 5.4. Overview of ν_e squared mass measurements.

Experiment	measured m^2 (eV ²)	limit (eV), 95% C.L.	Year
Mainz ¹¹⁰	$-0.6 \pm 2.2 \pm 2.1$	2.2	2004
Troitsk ¹¹¹	$-1.0 \pm 3.0 \pm 2.1$	2.5	2000
Mainz ¹¹²	$-3.7 \pm 5.3 \pm 2.1$	2.8	2000
LLNL ¹¹³	$-130 \pm 20 \pm 15$	7.0	1995
CIAE ¹¹⁴	$-31 \pm 75 \pm 48$	12.4	1995
Zurich ¹¹⁵	$-24 \pm 48 \pm 61$	11.7	1992
Tokyo INS ¹¹⁶	$-65 \pm 85 \pm 65$	13.1	1991
Los Alamos ¹¹⁷	$-147 \pm 68 \pm 41$	9.3	1991

is:

$$m_\beta = \sqrt{\sum_i |U_{ei}|^2 m_i^2}. \quad (5.21)$$

The simplest method for measuring neutrino mass is applied to the ν_μ . The mass is obtained from the 2-body decay-at-rest kinematics of $\pi \rightarrow \mu \nu_\mu$. One begins in the center of mass with the 4-vector relationship: $p_\pi = p_\mu + p_\nu$. Squaring and solving for neutrino mass gives: $m_\nu^2 = m_\pi^2 + m_\mu^2 - \sqrt{4m_\pi^2(|\mathbf{p}_\mu|^2 + m_\mu^2)}$. From this, one can see that this technique requires accurate measurement of the muon momentum, \mathbf{p}_μ , as well as the masses of the muon, m_μ and the pion, m_π . In fact, the uncertainty on the mass of the pion is what dominates the ν_μ mass measurement. As a result, a limit is set at $m_{\nu_\mu} < 170$ keV.^{107,108}

The mass for the ν_τ is obtained from the kinematics of τ decays. The τ typically decays to many hadrons. However, the four vectors for each of the hadrons can be summed. Then the decay can be treated as a two-body problem with the neutrino as one 4-vector and the sum of the hadrons as the other vector. At this point, the same method described for the ν_μ can be applied. Measurements are again error-limited, so a limit on the mass is placed. The best limit, which is $m_{\nu_\tau} < 18.2$ MeV, comes from fits to $\tau^- \rightarrow 2\pi^- \pi^+ \nu_\tau$ and $\tau^- \rightarrow 3\pi^- 2\pi^+ (\pi^0) \nu_\tau$ decays observed by the ALEPH experiment.¹⁰⁹

The experimental situation for the ν_e mass measurement is more complicated. The endpoint of the electron energy spectrum from tritium β decay is used to determine the mass. Just as in the case of the ν_μ and ν_τ , the experiments measure a value of m^2 . The problem is that the measurements have been systematically negative. A review of measurements, as a function of time, is given in Tab. 5.4. Recent measurements at Troitsk¹¹¹ and Mainz¹¹² are negative, but in agreement with zero. Following the Particle Data Group prescription for setting limit in the case of an unphysical

results, $m^2 = 0$ is assumed, with the quoted errors. Based on these results, one can extract a limit of approximately < 2 eV for the mass of the ν_e .

The next big step in the measurement of neutrino mass from decay kinematics will come from the Katrin Experiment.¹¹⁸ Katrin will use tritium beta decay to measure the mass of the neutrino to 0.2 eV. This does not reach the range of 0.05 eV, which our simplistic argument presented at the top of this section indicated. However, that argument assumed that the lightest neutrino had zero mass. A small offset from zero easily boosts the spectrum into the range observable by Katrin. On the other hand, Katrin is sensitive to only electron flavor. Thus, its sensitivity depends up on the amount of mixing of ν_e within the heaviest neutrino.

Another method for measuring neutrino mass from simple kinematics is to use time of flight for neutrinos from supernovae. Neutrinos carry away $\sim 99\%$ of the energy from a supernova. The mass limit is obtained from the spread in the propagation times of the neutrinos. The propagation time for a single neutrino is given by

$$t_{obs} - t_{emit} = t_0 \left(1 + \frac{m^2}{2E^2} \right) \quad (5.22)$$

where t_0 is the time required for light to reach Earth from the supernova. Because the neutrinos escape from a supernova before the photons, we do not know t_{emit} . But we can obtain the time difference between 2 events:

$$\Delta t_{obs} - \Delta t_{emit} \approx \frac{t_0 m^2}{2} \left(\frac{1}{E_1^2} - \frac{1}{E_2^2} \right). \quad (5.23)$$

using the assumption that all neutrinos are emitted at the same time, one can obtain a mass limit of ~ 30 eV from the ~ 20 events observed from SN1987a at 2 sites.^{119,120}

This is actually an oversimplified argument. The models for neutrino emission are actually quite complicated. The pulse of neutrinos has a prompt peak followed by a broader secondary peak with a long tail distributed over an interval which can be 4 s or more. The prompt peak is from “neutronization” and is mainly ν_e , while all three neutrino flavors populate the secondary peak. However, the rate of ν_e escape is slower compared to ν_μ and ν_τ produced at the same time, because the ν_e s can experience CC interactions, while the kinematic suppression from the charged lepton mass prevents this for the other flavors. However, when all of the aspects of the modeling are put together, the bottom line remains the same: it will be possible to set stringent mass limits if we observe neutrinos from nearby supernovae.

Some argue that cosmology provides a “direct measurement.” Cosmological fits have sensitivity to neutrino masses, but the results are dependent on the cosmological parameters¹²¹ and the model for relic neutrino production. There are many examples of models with low relic neutrino densities which would significantly change the present interpretation of the cosmological data.¹²² In the opinion of the author, until these issues are settled, cosmological measurements cannot convincingly compete with kinematic decays and supernova measurements, despite aggressive claims.

5.3. Neutrinos We Would Like to Meet

Now that we know that neutrinos have mass, and thus are outside of expectations, the obvious question is: “what other Beyond Standard Model properties do they possess?” *The APS Study on the Future of Neutrino Physics* focussed on this question. The plan for attack was divided into three fronts: (1) Neutrinos and the New Paradigm, (2) Neutrinos and the Unexpected and 3) Neutrinos and the Cosmos. The remainder of this paper follows this structure.

The consequences of the discovery of neutrino mass leads to a rich array of ideas. It is was beyond the scope of these lectures to cover the entire spectrum. So, in each of the three areas, two topics are chosen for extensive discussion. The reader is referred to the study¹ and the accompanying theory white paper² for further ideas.

5.3.1. *Neutrinos and the New Paradigm*

The first step in creating a “New Standard Model” is to incorporate neutrino mass. The simplest method is to introduce a Dirac mass, by analogy with the electron. This allows us to introduce a small neutrino mass, simply by arguing that the coupling to the Higgs is remarkably small. However, the unlikely smallness of the coupling has pushed theorists to look for other approaches. Among the oldest of these ideas is that neutrinos may be “Majorana particles,” *i.e.*, they are their own antiparticle. This leads to a new type of mass term in the Lagrangian. Through the “see-saw” mechanism, which fits well with Grand Unified Theories, this can also give a motivation for the apparently small value of the neutrino masses.

A direct consequence of the Majorana See-Saw Model is a heavy neutrino, with mass near the GUT scale. Because the heavy neutrino gets its mass through the Majorana rather than Dirac term of the Lagrangian, this

neutrino was massive during the earliest periods of the universe, before the electroweak phase transition. The decays of such a heavy lepton could be CP violating. This would provide a mechanism for producing the observed matter-antimatter imbalance seen today.

The tidiness of the the above theoretical ideas has caused this paradigm to emerge as the consensus favorite for the “New Standard Model.” However, there is absolutely no experimental evidence for this theory at this time. We have no evidence for the Majorana nature of neutrinos. Nor do we have any evidence for CP violation in the neutrino system. The great challenge of the next few years, then, is to find any sign at all that this theory is correct.

This section reviews how one introduces mass into the Lagrangian. The search for evidence of the Majorana nature of neutrinos though neutrinoless double beta decay is considered. Then, the prospects for finding evidence for CP violation is considered.

5.3.1.1. *How Neutrinos Might Get Their Mass*

The simplest assumption is that the neutrino mass should appear in the Lagrangian in the same way as for the charged fermions – via a Dirac mass term. In general, the Dirac mass term in the Lagrangian will be of the form

$$m(\bar{\psi}_L\psi_R + \bar{\psi}_R\psi_L). \quad (5.24)$$

From the arguments presented in eqs. 5.1 through 5.6, we saw that the scalar “mass” term mixes the RH and LH states of the fermion. If the fermion has only one chirality, then the Dirac mass term will automatically vanish. For this reason, a standard Dirac mass term for the neutrino will require the RH neutrino and LH antineutrino states.

To motivate the mass term, the most straightforward approach is to use the Higgs mechanism, as was done for the electron in the Standard Model. In the case of the electron, when we introduce a spin-0 Higgs doublet (h^0, h^+) , into the Lagrangian, we find terms like:

$$g_e\bar{\psi}_{eR}(\psi_{\nu L}(h^+)^{\dagger} + \psi_{eL}(h^0)^{\dagger}) + h.c., \quad (5.25)$$

where g_e is the coupling constant and “h.c.” is the Hermetian conjugate. The piece of this term proportional to $\bar{\psi}_{eR}\psi_{eL}(h^0)^{\dagger}$, combined with its Hermetian conjugate, can be identified with the Dirac mass term, $m_e\bar{\psi}_e\psi_e$. We set $\langle h^0 \rangle = v/\sqrt{2}$, so that we obtain $g\langle h^0 \rangle\bar{\psi}_e\psi_e$ and $m_e = g_ev/\sqrt{2}$. This is the Standard Model method for conveniently converting the *ad hoc*

electron mass, m_e , into an *ad hoc* coupling to the Higgs, g_e and a vacuum expectation value (VEV) for the Higgs, v . Following the same procedure for neutrinos allows us to identify the Dirac mass term with $m_\nu = g_\nu v / \sqrt{2}$. The VEV, v , has to be the same as for all other leptons. Therefore, the small mass must come from a very small coupling, g_ν . This implies that $g_e > 5 \times 10^4 g_\nu$.

There are several troublesome features to this procedure. The first issue which is often raised is:

- Why would the Higgs coupling vary across eleven orders of magnitude (the approximate ratio of the neutrino mass to the top quark mass)?

In fact, this question is rather odd. Disregarding the neutrinos, the masses of the charged fermions varies across six orders of magnitude (from the electron mass to the top mass). If six orders of magnitude do not bother anyone, why should eleven? Turning this around, if the Higgs couplings already seemed stretched in the charged fermion case, the neutrinos stretch the argument much further. This leads to the second troublesome issue,

- Physically, what is occurring?

The Higgs mechanism really gives little physical insight. While it does introduce mass, it has simply shifted the arbitrariness of the magnitude of the mass into an arbitrary coupling to a new field.

These two questions have led theorists to look at other explanations for small neutrino mass. It has been noted that neutrinos have the unique feature of carrying no electric or strong charge. Thus, neutrinos, alone among the Standard Model fermions, may be their own antiparticle, *i.e.* they may be Majorana particles. The nice consequence of this is a somewhat more motivated theory of mass for neutrinos.

To understand this, first consider what is meant to be a Dirac versus a Majorana particle. If neutrinos are Dirac particles, then the ν and the $\bar{\nu}$ are distinct particles, just as the electron and positron are distinct. The particle, ν has lepton number $+1$ and the antiparticle, $\bar{\nu}$ has lepton number -1 . Lepton number is conserved in an interaction. Thus, using the muon family as an example, ν_μ ($L = +1$) must produce μ^- ($L = +1$) and $\bar{\nu}_\mu$ ($L = -1$) must produce μ^+ ($L = -1$). The alternative viewpoint is that the ν and $\bar{\nu}$ are two helicity states of the same “Majorana” particle, which we can call “ ν^{maj} .” The π^+ decay produces the left-handed ν^{maj} and the π^- decay produces the right-handed ν^{maj} . This model explains all of the

data without invoking lepton number and has the nice feature of economy of total particles and quantum numbers, but it renders the neutrino different from all other Standard Model fermions.

Saying that the neutrino is its own antiparticle is equivalent to saying that the neutrino is its own charge conjugate, $\psi^c = \psi$. The operators which appear in the Lagrangian for the neutrino in this case are the set $(\psi_L, \psi_R, \psi_L^c, \psi_R^c)$ and $(\bar{\psi}_L, \bar{\psi}_R, \bar{\psi}_L^c, \bar{\psi}_R^c)$. Certain bilinear combinations of these in the Lagrangian can be identified as Dirac masses (*i.e.* $m(\bar{\psi}_L \psi_R + \dots)$). However, we also get a set of terms of the form:

$$(M_L/2)(\bar{\psi}_L^c \psi_L) + (M_R/2)(\bar{\psi}_R^c \psi_R) + \dots \quad (5.26)$$

These are the “Majorana mass terms,” which mix the pair of charge-conjugate states of the fermion. If the particle is not its own charge conjugate, then these terms automatically vanish and we are left with only the Dirac terms. Dirac particles have no Majorana mass terms, but Majorana particles will have Dirac mass terms.

The mass terms of the Lagrangian can be written in matrix form:

$$(1/2)(\bar{\psi}_L^c \quad \bar{\psi}_R) \begin{pmatrix} M_L & m \\ m & M_R \end{pmatrix} \begin{pmatrix} \psi_L \\ \psi_R^c \end{pmatrix} + h.c., \quad (5.27)$$

The Dirac mass, m , is on the off-diagonal elements, while the Majorana mass constants, M_L, M_R are on the diagonal. To obtain the physical masses, one diagonalizes the matrix.

One can now invoke “see-saw models” which motivate small observable neutrino masses. It turns out that GUT’s motivate mass matrices that look like:¹²⁴

$$\begin{pmatrix} 0 & m_\nu \\ m_\nu & M \end{pmatrix}, \quad (5.28)$$

with $m_\nu \ll M$. When you diagonalize this matrix to obtain the physical masses, this results in two states which can be measured experimentally:

$$m_{light} \approx m_\nu^2/M, \quad (5.29)$$

$$m_{heavy} \approx M \quad (5.30)$$

Grand Unified Theories favor very large masses for the “heavy neutrino” (often called a “neutral heavy lepton”). It is argued that it is most “natural” to have M be at the GUT scale. If $M \sim 10^{25} \text{ eV}$, and $m_{light} < 1 \text{ eV}$, as observed, then $m_\nu \sim 10^{12} \text{ eV}$, or is at the TeV scale. This is rather high compared to masses of other leptons, but not so far beyond the top quark mass to regard the connection as crazy. So while some arbitrariness

remains in this model, nevertheless there is a general feeling in the theory community that this is an improvement.

In this theory neutrinos have only approximate handedness, where the light neutrino is mostly LH with a very small admixture of RH and the neutral heavy lepton is essentially RH. Thus we have a LH neutrino which is light, which matches observations, and a RH neutrino which is not yet observed because it is far too massive.

5.3.1.2. Majorana vs. Dirac?

How can we experimentally tell the difference between the Dirac ($\nu, \bar{\nu}$) and Majorana (ν^{maj}) scenarios? One can imagine a straight-forward thought experiment. First, produce left-handed neutrinos in π^+ decays. These may be ν s or they may be ν_{LH}^{maj} s. Next, run the neutrino through a magic helicity-flipping device. If the neutrinos are Majorana, then what comes out of the flipping-device will be ν_{RH}^{maj} . These particles will behave like antineutrinos when they interact, showing the expected RH y -dependence for the cross section. But if the initial neutrino beam is Dirac, then what comes out of the flipping-device will be right-handed ν s, which are sterile. They do not interact at all. Such a helicity-flipping experiment is presently essentially impossible to implement. If neutrinos do have mass, then they may have an extremely tiny magnetic moment and a very intense magnetic field could flip their helicity. But the design requirements of such an experiment are far beyond our capability at the moment. Therefore, at the moment, we do not know if neutrinos are Majorana or Dirac in nature.

Instead, experimentalists are pursuing a different route. The Majorana nature of the neutrino can lead to an effect called neutrinoless double β decay: $(Z, A) \rightarrow (Z+2, A) + (e^- e^-)$. This is a beyond-the-Standard Model analogue to double β decay: $(Z, A) \rightarrow (Z+2, A) + (e^- e^- \bar{\nu}_e \bar{\nu}_e)$. Double β decay is a standard nuclear decay process with a very low rate because there is a suppression proportional to $(G_F \cos \theta_C)^4$. Therefore, in most cases, if the weak decay is possible, single β decay $((Z, A) \rightarrow (Z+1, A) + e^- + \bar{\nu}_e)$ will dominate. However, there are 13 nuclei, including $^{136}\text{Xe} \rightarrow ^{136}\text{Ba}$ and $^{76}\text{Ge} \rightarrow ^{76}\text{Se}$, for which single β decay is energetically disallowed. In these cases double β decay with two neutrinos has been observed.¹²³ If the neutrino were its own antiparticle, then the neutrinos produced in the double β decay process could annihilate, yielding neutrinoless double β decay.

If there are Majorana neutrinos, then the amplitude for $0\nu\beta\beta$ is propor-

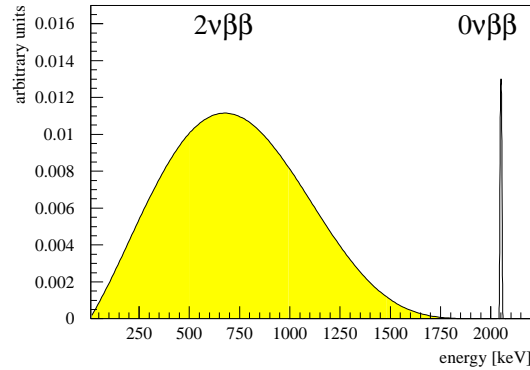


Fig. 5.16. Spectrum for two-neutrino double β decay and expected peak for neutrinoless double β decay.

tional to the square of

$$m_{0\nu\beta\beta} = \sum U_{ei}^2 m_i. \quad (5.31)$$

This should be contrasted with eq. 5.21. The $0\nu\beta\beta$ searches are probing different effective masses than the direct searches and the two results yield complementary information. Like the direct searches, the possibility of seeing $0\nu\beta\beta$ depends on the amount of electron-flavor mixed in the most massive neutrino state. If this is small, then the rate of decay will be very low. Thus the hierarchy of the neutrino states affects our ability to observe $0\nu\beta\beta$. To completely untangle the Dirac *vs.* Majorana question, three different experiments – direct mass measurement, hierarchy measurement and $0\nu\beta\beta$ measurement – may be required.²

Extracting $m_{0\nu\beta\beta}$ from a measured half-life leads to a theoretical error from the nuclear matrix element calculations. A favored style of calculation uses the “QRPA” (Quasiparticle Random Phase Approximation)^{125–128} model. Using ^{100}Mo as an example, different matrix elements from QRPA calculations cause $m_{0\nu\beta\beta}$ to vary by up to 2 eV for a half-life of 4.5×10^{23} years.¹²⁹ So the error is significant.

The $0\nu\beta\beta$ events must be separated from the standard two-neutrino double β ($2\nu\beta\beta$) decay background. This can be done through simple kinematics cuts. The two-body nature of $0\nu\beta\beta$ decay will cause a peak at

the endpoint of the $2\nu\beta\beta$ decay (4-body) spectrum, as shown in Fig. 5.16. An advantage of observing $2\nu\beta\beta$, however, is that measurement of its half-life allows direct measurement of the matrix element. At this point the $2\nu\beta\beta$ decay spectrum has been observed in 10 elements. In some cases, such as ^{100}Mo , the $2\nu\beta\beta$ half-life is well measured and can be used to constrain nuclear matrix element calculation. For this case, NEMO-3 reports a half life of $(7.68 \pm 0.02(\text{stat}) \pm 0.54(\text{sys})) \times 10^{18} \text{ y}$.¹³⁰

At present, no signal for $0\nu\beta\beta$ decay has been clearly observed. The present 90% CL limit on the lifetime from CUORICINO on ^{130}Te is 1.8×10^{24} years, corresponding to limit of $m_{0\nu\beta\beta} < 0.2 - 1.1 \text{ eV}$.¹³¹ The NEMO-3 experiment has set 90% CL limits of 4.6×10^{23} and 1.0×10^{23} on ^{100}Mo and ^{82}Se , respectively.¹²⁹ The corresponding limits on $m_{0\nu\beta\beta}$ are 0.7-2.8 eV and 1.7-4.9 eV.¹²⁹ There is a candidate signal observed at 4.2σ from a Germanium detector,¹³² although the statistical significance is under debate.² The measured half-life was 1.19×10^{25} years. Until this result is confirmed by further experiments, it is best to reserve judgment.

Luckily, a range of future $0\nu\beta\beta$ decay experiments are on the horizon. These are expected to probe an order of magnitude further in lifetimes. In particular, the germanium-based GERDA experiment,¹³³ will turn on soon and will address the existence of the possible signal. CUORE,¹³⁴ SuperNEMO,¹³⁵ EXO,¹³⁶ Majorana¹³⁷ and Moon¹³⁸ will extend the search even further using a wide range of elements. The reach of these near future $0\nu\beta\beta$ covers the prediction for the inverted mass hierarchy.

5.3.1.3. *CP Violation in the Neutrino Sector*

An intriguing aspect of the “new Standard Model” is the heavy GUT-scale neutrinos which gain mass through the Majorana terms in the Lagrangian. There could be more than one, and likely, given the trend in the Standard Model, there would be three, so we can label these N_1 , N_2 and N_3 . These heavy neutrinos have mass prior to the electroweak phase transition in which the Dirac terms appear. As a result, prior to the electroweak phase transition, decays shown in Fig. 5.17 are possible. Both decays produce the same final state, $N_1 \rightarrow \ell H$, where ℓ and H are oppositely charged. These diagrams interfere, and can lead to a different decay rate to ℓ^- and ℓ^+ , which is CP violation.

This form of CP violation would lead to a lepton asymmetry in the early universe which could be transferred into a baryon asymmetry. A mechanism for this already appears in the Standard Model, in which but B , baryon

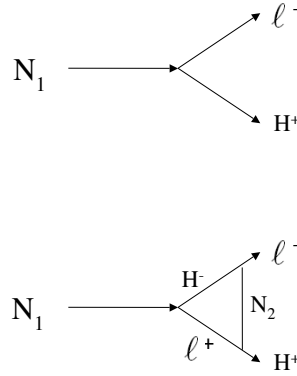


Fig. 5.17. Example of two diagrams for Neutral Heavy Lepton decay which can interfere to produce CP violation.

number, and L , lepton number are not conserved, but the difference, $B - L$, is exactly conserved. B and L violation occurs in transitions between vacuum states at high energies, called the “sphaleron process.” Variations on this mechanism, called “leptogenesis,” may explain the matter-antimatter asymmetry we see today.

N_1 , N_2 , and N_3 are far too massive to be produced at accelerators in the near future. Thus observing CP violation in their decays is out of the question. However, observing CP violation in the light neutrino sector would be a plausible hint that the theory is correct.

To incorporate CP violation into the three-light-neutrino model, the leptonic mixing matrix is expanded and written as: $U^{with\ CP} = VK$. In this case, V is very similar to the U of Eq. 5.12, but with a CP violating phase, δ :

$$V = \begin{pmatrix} c_{12}c_{13} & s_{12}c_{13} & s_{13}e^{-i\delta} \\ -s_{12}c_{23} - c_{12}s_{23}s_{13}e^{i\delta} & c_{12}c_{23} - s_{12}s_{23}s_{13}e^{i\delta} & s_{23}c_{13} \\ s_{12}s_{23} - c_{12}c_{23}s_{13}e^{i\delta} & -c_{12}s_{23} - s_{12}c_{23}s_{13}e^{i\delta} & c_{23}c_{13} \end{pmatrix}. \quad (5.32)$$

This is analogous to the CKM matrix of the quark sector. The other term,

$$K = \text{diag}(1, e^{i\phi_1}, e^{i(\phi_2+\delta)}) \quad (5.33)$$

has two further CP violating phases, ϕ_1 and ϕ_2 .

Now, we potentially have three non-zero CP violating parameters in the light neutrino sector, δ , ϕ_1 and ϕ_2 , as well as one or more CP violating parameters in the heavy neutrino sector, where the number depends upon the total number of N . In the Lagrangian, these all come from a matrix of Yukawa coupling constants. In principle, all of these phases can take on the full range of values, including exactly zero. However, it is difficult to motivate a theory in which some are nonzero and some are exactly zero. It is expected that these parameters will either all have non-zero values or all be precisely zero. If the latter case, then the difference between the lepton sector, with no CP violation, and quark sector, with clear CP violation, must be motivated. As a result, observation of CP violation in the light neutrino sector is regarded as the “smoking gun” to CP violation in the heavy sector.

Returning to the light neutrino sector, how can the CP phases be measured? The ϕ phases arise as a direct consequence of the Majorana nature of neutrinos. Therefore, in principle, the ϕ phase associated with the electron family is accessible in neutrinoless double beta decay. In practice, this will be extremely hard to measure because this term manifests itself as a change in the sum in eq. 5.31, which is proportional to the $0\nu\beta\beta$ decay amplitude. Thus one seeks to measure a deviation of the (as-yet-unmeasured) $0\nu\beta\beta$ lifetime from the prediction which depends upon the mixing angles (with relatively large errors at present), the (unknown) neutrino masses, and the (poorly known) nuclear matrix element. Even if the effect is large, observation of the effect is clearly hopeless in the near future. On the other hand, δ , the “Dirac” CP violating term in V may be accessible through oscillation searches.

CP violation searches involve observing a difference in oscillation probability for neutrinos and antineutrinos. Only appearance experiments can observe CP violation. A difference between oscillations of neutrinos and antineutrinos in disappearance searches is CPT violating. In oscillation appearance searches, the K matrix does not affect the oscillation probability because this diagonal matrix is multiplied by its complex conjugate. On the other hand, non-zero δ can be observed. To test for non-zero δ , the oscillation probability must depend upon the U_{e3} component of Eq. 5.32. In other words, the search needs to involve transitions from or to electron flavor and

involve the mass state ν_3 . This combination of requirements – appearance signal, electron flavor involvement, and ν_3 mass state involvement – leads to one experimental option at present: comparison of $\nu_\mu \rightarrow \nu_e$ to $\bar{\nu}_\mu \rightarrow \bar{\nu}_e$ at the atmospheric Δm^2 , which is Δm_{13}^2 . The oscillation probability is given by:

$$\begin{aligned}
 P_{long-baseline} &\simeq \sin^2 2\theta_{13} \sin^2 \theta_{23} \sin^2 \Delta \\
 &\mp \alpha \sin 2\theta_{13} \sin \delta_{CP} \cos \theta_{13} \sin 2\theta_{12} \sin 2\theta_{23} \sin^3 \Delta \\
 &+ \alpha \sin 2\theta_{13} \cos \delta_{CP} \cos \theta_{13} \sin 2\theta_{12} \sin 2\theta_{23} \cos \Delta \sin^2 \Delta \\
 &+ \alpha^2 \cos^2 \theta_{23} \sin^2 2\theta_{12} \sin^2 \Delta,
 \end{aligned} \tag{5.34}$$

where α and Δ are defined in eq. 5.20. The second term is negative for neutrino scattering and positive for antineutrino scattering.

Unfortunately, eq. 5.34 convolutes two unknown parameters, the sign of Δm_{13}^2 (the mass hierarchy) and the value of θ_{13} , with the parameter, δ , that we want to measure. The problem of the mass hierarchy can be mitigated by the experimental design. The sign of $\Delta m_{13}^2 = m_3^2 - m_1^2$ affects the terms where Δm^2 is not squared. These terms arise from matter effects and can so be reduced if the pathlength in matter is relatively short. For long baseline experiments, which must shoot the beam through the Earth, this means that L must be relatively short. In order to retain the same L/E and, hence, the same sensitivity to Δm_{13}^2 , E must be comparably reduced. On the other hand, the problem of θ_{13} cannot be mitigated. From eq. 5.32, one sees that we are in the unfortunate situation of having the CP violating term multiplied by $\sin \theta_{13}$. The smaller this factor, the harder it will be to extract δ . If $\sin^2 2\theta_{13}$ is smaller than ~ 0.01 at 90% CL, then substantial improvements in beams and detectors will be required.

Eq. 5.34 also depends on two other as-yet-poorly understood parameters, θ_{23} and the magnitude of Δm_{23}^2 . Disappearance experiments measure $\sin^2 2\theta_{23} = 1.00^{+0.16}_{-0.14}$,⁶⁷ thus there is an ambiguity as to whether θ_{23} is larger or smaller than 45° . Δm_{23}^2 is only known to about 10%.^{56,67} This measurement is extracted from the location of the “dip” in the rate versus L/E distribution of disappearance experiments, and is already systematics-dominated. Improvement requires experiments with better energy resolution⁵⁶ and better understanding of the CCQE and background cross sections.¹³⁹ These errors lend a significant error to the analysis.

Lastly, it is difficult to measure a ν_e signal which is at the $\sim 1\%$ level. Most ν_μ beams have a substantial ν_e intrinsic contamination from μ and K decays. Given that θ_{13} is small, this contamination is a serious issue.

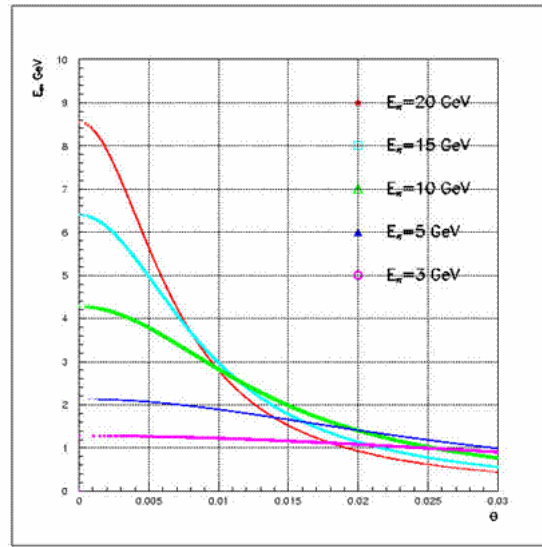


Fig. 5.18. Neutrino energy versus angle off-axis for various values of pion energy. In this example one can see that for moderate off-axis angles, between 15-30 mrad, all pion energies between 3 and 20 GeV map to approximately 1 GeV neutrino energy.

One solution to this problem is to go to an off-axis beam design. This relies on the tight correlation between energy and off-axis angle, θ , in two-body decays. For pion decay, which dominates most beams,

$$E_\nu = \frac{0.43E_\pi}{1 + \gamma^2\theta^2}, \quad (5.35)$$

where $\gamma = E_\pi/m_\pi$ is the Lorentz boost factor. The solution for two-body K decay replaces 0.43 with 0.96. Thus at $\theta = 0$, the relationship between E_ν and E_π is linear. However, for larger θ , above a moderate energy threshold, all values of E_π map to the same E_ν . This is illustrated in Fig. 5.18. The result is that an off axis ν_μ beam which comes largely from pion decay is tightly peaked in energy while the ν_e intrinsic background is spread across a range of energies. This also helps to reduce ν_μ events which are mis-

reconstructed as ν_e scatters, such as NC π^0 production where a photon is lost. These “mis-ids” tend to be spread across a range of energies, since the true energy is misreconstructed. Thus a peaked signal, as one expects from an off-axis beam, is helpful in separating signal and background.

The major problem with this design is that off axis beams have substantially lower flux. The flux scales¹⁴⁰ as:

$$F = \left(\frac{2\gamma}{1 + \gamma^2 \theta^2} \right)^2 A / 4\pi z^2. \quad (5.36)$$

In this equation, A is the area of the detector and z is the distance to the detector. Two future long baseline experiments, NOvA⁴⁰ and T2K¹⁴¹ are proposing off-axis beams for a $\nu_\mu \rightarrow \nu_e$ search. Because of the low flux, very large detectors are required.

In summary, the path to a test for non-zero δ is clear but will take several steps and requires some luck. First, a clean measure θ_{13} from Double Chooz and Daya Bay is needed. If $\sin^2 2\theta_{13} < 0.005$ at 90% CL, then a significant measurement of CP violation is unlikely to be possible in the near future. At the same time, improvements in the θ_{23} and Δm_{23}^2 from disappearance ($\nu_\mu \rightarrow \nu_\mu$) measurements at MINOS and T2K will improve the situation. T2K and NOvA⁴⁰ may be able to make a first exploration of CP parameter space, from ν_e appearance measurements, depending on statistics. NOvA may also be able to address the mass hierarchy question. This will open up the possibility of measuring CP violation to the next generation of very long baseline experiments.¹⁴² The most sensitive of these use a beam originating at Fermilab and a LAr detector located at Ash River, Minnesota⁴⁵ or a Cerenkov or LAr detector located at the Deep Underground Science Laboratory at Homestake.¹⁴³

At some point in the future, a beta beam or a neutrino factory beam could provide an intense source of ν_e and $\bar{\nu}_e$ fluxes, allowing comparison of $\nu_e \rightarrow \nu_\mu$ to $\bar{\nu}_e \rightarrow \bar{\nu}_\mu$. In this case one would search for events with wrong-sign muons in a calorimeter-style detector. This would be a striking signature with low background, especially in the case of a beta beam. This could allow a very precise measurement of δ .¹⁴⁴

5.3.2. Neutrinos and the Unexpected

While it is nice to have a tidy, well-motivated theory of neutrino masses, it is disconcerting to have essentially no experimental evidence for this theory. Moreover, neutrino theories have a history of being incorrect. Only a decade ago, most theorists would have told you that neutrinos have no mass. Those

who thought neutrinos might have mass believed it would be relatively large (> 5 eV), explaining dark matter. Most theorists also believed that if the solar neutrinos were experiencing oscillations, the correct solution would be the small mixing angle MSW solution, because the mixing matrix should look like the quark matrix. Using the same logic, the atmospheric neutrino deficit, which could only correspond to large mixing angle, was routinely dismissed as an experimental effect.

On the basis of this, it is wise not to constrain ourselves to the “New Paradigm.” The reason the APS neutrino study chose to devote a chapter to “the Unexpected” was to emphasize the importance of being open to what nature is telling us about neutrinos. There are two ways to approach this idea: (1) the theory-driven approach: explore for properties which could, theoretically, exist and (2) the experiment-driven approach: follow up on anomalous results which have been observed.

For lack of time, I will only briefly consider two examples of the first case: searching for a neutrino magnetic moment and searching for CPT violation. In the Standard Model, the neutrino magnetic moment is expected to be $\sim 10^{-19} \mu_B$. Laboratory experiments and astrophysical limits are many orders of magnitude away from this level.¹⁴⁵ Nevertheless, if a new experiment could advance this measurement by an order of magnitude, that would be worth pursuing. A more startling discovery would be a difference in the oscillation disappearance probability of neutrinos versus antineutrinos. In a three-neutrino model, a difference in the rate of disappearance of neutrinos and antineutrinos would imply CPT violation. MINOS will be the next experiment to pursue such a search.³⁶ If CPT violation were discovered we would need to rethink the very basis of our theory. However, there are theorists exploring these ideas.

The remainder of this section will focus on the second approach, exploring “anomalies” which have appeared in various experiments. Physicists today are always cautious about pursuing deviations from the Standard Model. Most do not, in the end, point to new physics. The Standard Model has been very resilient. Most anomalies are arguably more likely due to systematic effects or statistical fluctuations, than to new physics. However, those which do “pan out” completely change the way we think. The solar neutrino deficit is a perfect example. So, if a new, unexpected result withstands questions by the community on the systematics of the experiment, then the anomaly becomes worth pursuing further.

There are several examples of $> 3\sigma$ unexpected results in the neutrino sector which are worth pursuing and two cases are covered here. The first,

the LSND anomaly, is being actively pursued. The second, the NuTeV anomaly, will require a new experiment. Unlike most of the topics in these lectures, the NuTeV anomaly is not directly related to neutrino oscillations and neutrino mass, and so expands the discussion, which has so far been rather narrowly focussed.

Along with the known discrepancies which have reached the level of full-fledged anomalies, there are also examples of “unexpected results to watch.” These results which have not yet reached the 3σ level, but are showing interesting trends. For example, unconstrained fits to atmospheric oscillation data from a wide range of experiments consistently result in $\sin^2 2\theta_{23}$ best fit value greater than unity. While in each case, the best fit is $\sim 1\sigma$ from unity, it is the trend which is interesting, since the experiments involved are all very different. There is simply not enough space to cover this and other examples of “results to watch.”

The take-away message of this section is: the neutrino sector is a rich place for new physics to appear, and physicists need to be alert and open-minded to what nature is saying.

5.3.2.1. The LSND Anomaly

The LSND experiment ran at the LAMPF accelerator at Los Alamos National Laboratory between 1993 and 1998. The decay-at-rest (DAR) beam was produced by impinging 800 MeV protons on a beam dump. These produced π^+ s which stop and decay to produce μ^+ s, which also stop and decay to produce $\bar{\nu}_\mu$ and ν_e . These were studied in the range of 20 to 55 MeV. The π^- s capture, so the beam has a $< 8 \times 10^{-4}$ contamination of $\bar{\nu}_e$. The neutrino events were observed in a detector located 30 m downstream of the beam dump. 1220 phototubes surrounded the periphery of a cylindrical detector filled with 167 tons of mineral oil, lightly doped with scintillator. The signature of a $\bar{\nu}_e$ appearance was $\bar{\nu}_e + p \rightarrow e^+ n$. This resulted in a two-component signature: the initial Cerenkov and scintillation light associated with the e^+ , followed later by the scintillation light from the n capture on hydrogen, producing a 2.2 MeV γ . The experiment observed $87.9 \pm 22.4 \pm 6.0$ events, a 4σ excess¹⁴⁶ above expectation.

LSND is a short baseline experiment, with an $L/E \sim 1$ m/MeV. Thus, from the two-generation oscillation formula, eq. 5.10, one can see that this experiment is sensitive to $\Delta m^2 \geq 0.1$ eV². Other experiments have searched for oscillations at high Δm^2 , and the two most relevant to LSND are Karmen¹⁴⁷ and Bugey.¹⁴⁸ The KARMEN experiment, which also used a DAR

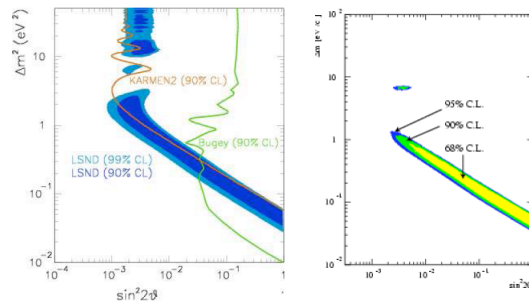


Fig. 5.19. Left: LSND allowed range compared to short baseline experiment limits. Right: Allowed range from the Karmen-LSND joint analysis.¹⁴⁹

muon beam and was located 17.7 m from the beam dump, had sensitivity to address only a portion of the LSND region, and did not see a signal there. Since the design of the experiments are very similar, one can think of the Karmen experiment as a “near detector,” which measures the flux before oscillation. The results were combined in a joint analysis performed by collaborators from both experiments; the allowed range for oscillations is shown in Figure 5.19.¹⁴⁹ The Bugey experiment was a reactor-based $\bar{\nu}_e$ disappearance search which set a limit on oscillations. Because this is disappearance and not explicitly $\bar{\nu}_e \rightarrow \bar{\nu}_\mu$, its limit is applicable to LSND in many, but not all, oscillation models. This limit is shown in Figure 5.19.

Why can’t we fit LSND into the three-neutrino theory? The LSND signal cannot be accommodated within the standard three-neutrino picture, given the solar and atmospheric oscillations. To see the incompatibility, first consider the case where the oscillation signals de-couple into, effectively, two-generation oscillations (eq. 5.10). For three generations, then $\Delta m_{31}^2 = \Delta m_{32}^2 + \Delta m_{21}^2$, which is clearly not the case for these three signals. The more general case allows the atmospheric result to be due to a mixture of high (LSND-range) and low (solar-range) Δm^2 values. In order for this model to succeed, the atmospheric Δm^2 from a shape

Table 5.5. Results used in 3+2 fit. $\sin^2 2\theta$ limit is 90% CL

Channel	Experiment	Lowest Δm^2	$\sin^2 2\theta$ at high Δm^2	Best reach in $\sin^2 2\theta$
$\nu_\mu \rightarrow \nu_e$	LSND	0.03 eV ²	$> 2.5 \times 10^{-3}$	$> 1.2 \times 10^{-3}$
	KARMEN	0.06 eV ²	$< 1.7 \times 10^{-3}$	$< 1.0 \times 10^{-3}$
	NOMAD	0.4 eV ²	$< 1.4 \times 10^{-3}$	$< 1.0 \times 10^{-3}$
ν_e disappearance	Bugey	0.01 eV ²	$< 1.4 \times 10^{-1}$	$< 1.3 \times 10^{-2}$
	Chooz	0.0001 eV ²	$< 1.0 \times 10^{-1}$	$< 5 \times 10^{-2}$
ν_μ disappearance	CCFR84	6 eV ²	NA	$< 2 \times 10^{-1}$
	CDHS	0.3 eV ²	NA	$< 5.3 \times 10^{-1}$

analysis must shift up from its present value of $\sim 2 \times 10^{-3}$ eV² and the chlorine experiment must have overestimated the deficit of ⁷Be solar neutrinos. However, the largest clash between data and this model arises from the Super-K ν_e events. This model requires that Super-K has missed a ν_e appearance signal of approximately the same size and shape as the ν_μ deficit before detector smearing and cuts. Neutrino measurements are experimentally difficult and parameters do sometimes shift with time as systematics are better understood, but it seems unlikely that all of the above results could change sufficiently to accommodate LSND.

Sterile Neutrinos as a Solution Additional neutrinos which do not interact via exchange of W or Z are called “sterile;” they may mix with active neutrinos, and thereby can be produced in neutrino oscillations. Experimental evidence of this would be the disappearance of the active flavor from the beam. In contrast to the GUT-scale sterile neutrinos we have already discussed, the sterile neutrinos which could explain LSND must be light (in the eV range), and this narrows the class of acceptable theories. Nevertheless, a number of possible explanations remain.¹⁵⁰

Sterile neutrinos solve the LSND problem by adding extra mass splittings. The additional mass states must be mostly sterile, with only a small admixture of the active flavors in order to accommodate the limits on sterile neutrinos from the atmospheric and solar experiments. In principle, one might expect three sterile neutrinos. In practice, the data cannot constrain information on more than two sterile neutrinos. Therefore these are called “3+2” models. The method for fitting the data is described in reference.¹⁵¹ One is fitting for two additional mass splittings, Δm_{14}^2 and Δm_{15}^2 . In the fit, the three mostly active neutrinos are approximated as degenerate. The mixing matrix is also expanded by two rows and two columns.

The data that drive the fits are the “short baseline” experiments that

provide information on high Δm^2 oscillations, summarized in Tab. 5.5. The combination of $\bar{\nu}_\mu \rightarrow \bar{\nu}_e$ (LSND,¹⁴⁶ Karmen II¹⁴⁷), $\nu_\mu \rightarrow \nu_e$ (NO-MAD¹⁵²), ν_μ disappearance (CDHS,¹⁵³ CCFR84¹⁵⁴), and ν_e disappearance (Bugey,¹⁴⁸ CHOOZ²⁵) must all be accommodated within the model. A constraint for Super K ν_μ disappearance is also included. None of the short baseline experiments except for LSND provide evidence for oscillations beyond 3σ . However, it should be noted that CDHS has a 2σ (statistical and systematic, combined) effect consistent with a high Δm^2 sterile neutrino when the data are fit for a shape dependence, and Bugey has a 1σ pull at $\Delta m^2 \sim 1\text{eV}^2$. As a result, these two experiments define the best fit combination of high and low Δm^2 for the 3+2 model. However, there are acceptable solutions with a combination of low Δm^2 values. The best fit,¹⁵¹ has $\Delta m_{14}^2 = 0.92\text{ eV}^2$, $\Delta m_{15}^2 = 22\text{ eV}^2$, although there are combinations which work with two relatively low Δm^2 values. A wide range of mixing angles can be accommodated, and the best fit has $U_{e4} = 0.121$, $U_{\mu 4} = 0.204$, $U_{e5} = 0.036$ and $U_{\mu 4} = 0.224$. The other mixing angles involving the sterile states are not probed by the ν_μ disappearance, ν_e disappearance and $\nu_\mu \rightarrow \nu_e$ appearance experiments listed above. There is 30% compatibility for all other experiments and LSND.

Introducing extra neutrinos, including sterile ones, would have cosmological implications, compounded if the extra neutrinos have significant mass ($>1\text{ eV}$). However, there are several ways around the problem. The first is to note that while the best fit requires a high mass sterile neutrino, there are low-mass fits which work within the 3+2 model. The second is to observe that there are a variety of classes of theories where the neutrinos do not thermalize in the early universe.¹²² In this case, there is no conflict with the cosmological data, since the cosmological neutrino abundance is substantially reduced.

If more than one Δm^2 contributes to an oscillation appearance signal, then the data can be sensitive to a CP-violating phase in the mixing matrix. Experimentally, for this to occur, the Δm^2 values must be within less than about two orders of magnitude of one another.

In 3+2 CP-violating models:¹⁵⁵

$$\begin{aligned}
 P(\nu_{\mu}^{(-)} \rightarrow \nu_e^{(-)}) = & 4|U_{e4}|^2|U_{\mu4}|^2 \sin^2 x_{41} \\
 & + 4|U_{e5}|^2|U_{\mu5}|^2 \sin^2 x_{51} \\
 & + 8|U_{e4}||U_{\mu4}||U_{e5}||U_{\mu5}| \\
 & \sin x_{41} \sin x_{51} \cos(x_{54} \mp \phi_{54}),
 \end{aligned} \tag{5.37}$$

where in the last line, the negative sign is for neutrino oscillations and the positive sign is for antineutrino oscillations, and defined:

$$x_{ji} \equiv 1.27 \Delta m_{ji}^2 L/E, \quad \phi_{54} \equiv \arg(U_{e4}^* U_{\mu4} U_{e5} U_{\mu5}^*).$$

Thus the oscillation probability is affected by CP violation through the term ϕ_{54} . The CP conserving cases are $\phi_{54} = 0$ and 180 degrees.

MiniBooNE First Results The main purpose of the MiniBooNE experiment was to resolve the question of the LSND signal. First results of this experiment, presented in April, 2007, considered those explanations with a high expectation for $\nu_{\mu} \rightarrow \nu_e$ oscillations. This includes the CP conserving 3+2 model and many cases of CP violating 3+2 models described above. As will be described below, the first results are incompatible with $\nu_{\mu} \rightarrow \nu_e$ oscillations, but show an unexpected low energy excess, very much in keeping with the subsection title of “Neutrinos and the Unexpected.”

The MiniBooNE experiment uses the Fermilab Booster Neutrino Beam, which is produced from 8 GeV protons incident on a beryllium target located within a magnetic focusing horn. The current of the horn can be reversed such that the beam is dominantly neutrinos or antineutrinos. The first results are from neutrino running. The MiniBooNE detector is located $L = 541$ m from the primary target, and the neutrino flux has average energy of ~ 0.75 GeV. The detector is located 541 m from the front of the beryllium target and consists of a spherical tank of radius 610 cm that is covered on the inside by 1520 8-inch photomultiplier tubes and filled with 800 tons of pure mineral oil (CH_2). Neutrino events in the detector produce both Cerenkov and scintillation light.

In order to test the LSND result, the MiniBooNE design maintains $L/E \sim 1$ m/MeV while substantially changing the systematic errors associated with the experiment. This is accomplished by increasing both L and E by an order of magnitude from the LSND design. This changes the source of the neutrinos (ν_{μ} from energetic pions rather than $\bar{\nu}_{\mu}$ from

stopped muons), the signature for the signal, and the major backgrounds in the detector. In its first run, in neutrino mode, MiniBooNE collected over a million clean, neutrino events. About 99.5% of the MiniBooNE neutrino events are estimated to be ν_μ -induced, while 0.5% are estimated to be due to “intrinsic” ν_e background in the beam.

The initial MiniBooNE results were analyzed within an appearance-only, two neutrino oscillation context. While the LSND signal must be a result of a more complex oscillation model, in most cases a $\nu_\mu \rightarrow \nu_e$ -like oscillation signal is predicted. After the complete ν_e event selection is applied, the total background was estimated to be 358 ± 35 events, while 163 ± 21 signal events were expected for the LSND central expectation of 0.26% $\nu_\mu \rightarrow \nu_e$ transmutation.

The top plot of Fig. 5.20 shows candidate ν_e events as a function of reconstructed neutrino energy (E_ν^{QE}). The vertical dashed line indicates the minimum E_ν^{QE} used in the two-neutrino oscillation analysis. There is no significant excess of events ($22 \pm 19 \pm 35$ events) for $475 < E_\nu^{QE} < 1250$ MeV; however, an excess of events ($96 \pm 17 \pm 20$ events) is observed below 475 MeV. In the top plot, the points show the statistical error, while the histogram is the expected background with systematic errors from all sources. The background subtracted excess as a function of E_ν^{QE} is shown in the bottom plot, where the points represent the data with total errors. Oscillation scenarios are indicated by the histograms.

The low-energy excess cannot be explained by a two-neutrino oscillation model, and its source is under investigation. The low energy events isolated by the cuts, including the excess events, are single-ring and electromagnetic-like, with no unusual detection issues. The low energy excess events are neither consistent with the spatial nor energy distributions of photons coming from interactions outside of the tank. Nor are they consistent with the energy distribution from single photons from radiative Δ decays ($\Delta \rightarrow N + \gamma$). Mis-identification of π^0 events is well constrained in MiniBooNE by the rate of reconstructed π^0 events, studied as a function of π^0 momentum.¹⁵⁶ This rate would need to be mis-measured by well over a factor of three to explain the excess, far outside of the error of the analysis.

With that said, as shown in Fig. 5.20, the excess is not in agreement with a simple two-neutrino $\nu_\mu \rightarrow \nu_e$ oscillation signal. This figure shows the predicted spectrum when the best-fit two-neutrino oscillation signal is added to the predicted background. The bottom panel of the figure shows background-subtracted data with the best-fit two-neutrino oscillation and two oscillation points from the favored LSND region.

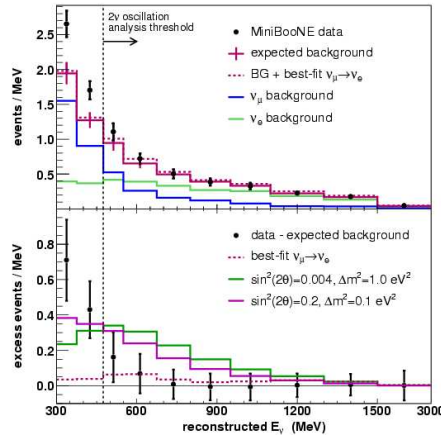


Fig. 5.20. The top plot shows the number of candidate ν_e events as a function of E_ν^{QE} . Also shown are the best-fit oscillation spectrum (dashed histogram) and the background contributions from ν_μ and ν_e events. The bottom plot shows the number of events with the predicted background subtracted as a function of E_ν^{QE} . The two histograms correspond to LSND solutions at high and low Δm^2 .

A single-sided raster scan to a two neutrino appearance-only oscillation model is used in the energy range $475 < E_\nu^{QE} < 3000$ MeV to find the 90% CL limit corresponding to $\Delta\chi^2 = \chi_{limit}^2 - \chi_{bestfit}^2 = 1.64$. As shown by the top plot in Fig. 5.21, the LSND 90% CL allowed region is excluded at the 90% CL. A joint analysis as a function of Δm^2 , using a combined χ^2 of the best fit values and errors for LSND and MiniBooNE, excludes at 98% CL two-neutrino appearance-only oscillations as an explanation of the LSND anomaly. The bottom plot of Fig. 5.21 shows limits from the KARMEN¹⁴⁷ and Bugey¹⁴⁸ experiments. This plot represents an example of the problem of apples-to-apples comparisons raised in sec. . The MiniBooNE and Bugey curves are 1-sided upper limits on $\sin^2 2\theta$ corresponding to $\Delta\chi^2 = 1.64$ – hence directly comparable – while the published KARMEN curve is a “Feldman Cousins” contour.

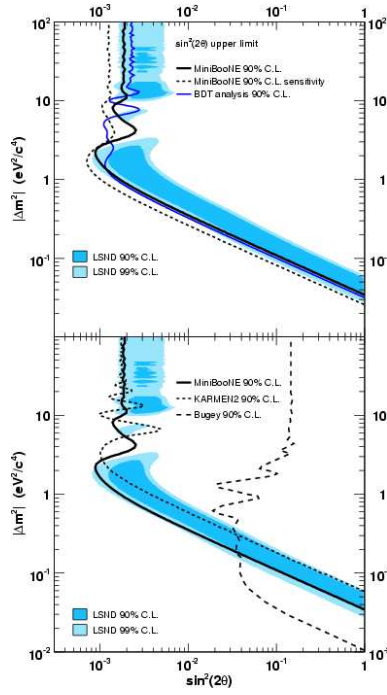


Fig. 5.21. The top plot shows the $\nu_\mu \rightarrow \nu_e$ MiniBooNE 90% CL limit (thick solid curve) and sensitivity (dashed curve) for events with $475 < E_\nu^{QE} < 3000$ MeV. Also shown is the limit from a second cross-check analysis (thin solid curve). The bottom plot shows the limits from the KARMEN¹⁴⁷ and Bugey¹⁴⁸ experiments. The shaded areas show the 90% and 99% CL allowed regions from the LSND experiment.

Next Steps From the initial MiniBooNE result, one can draw two conclusions: (1) there is excellent agreement between data and prediction in the analysis region originally defined for the two-neutrino oscillation search and (2) there is a presently unexplained discrepancy with data lying above background at low energy. This combination of information severely limits models seeking to explain the LSND anomaly.

Interpreting the MiniBooNE data as appearance-only and combining this result with other data in a 3+2 fit does not give a satisfactory result.¹⁵⁷ While MiniBooNE and LSND are compatible if CP violation is allowed in the 3+2 model, there is tension between these results and the ν_μ disappearance experiments. This might be addressed if a 3+2 interpre-

tation of the MiniBooNE result were expanded to include the possibility of ν_μ disappearance and intrinsic ν_e disappearance. This analysis is underway by the MiniBooNE collaboration.¹⁵⁸ Most likely, if a good fit is obtained in a 3+2 scenario, it will require some level of CP violation. MiniBooNE is presently collecting data in antineutrino mode. However, this is a small data set ($\sim 2 \times 10^{20}$ protons on target producing the beam) and future running to reach roughly three times the statistics will be required to make a decisive statement. Other, alternative explanations are also being explored^{159–161}.

An upcoming result which will shed light on the question is the analysis of the MiniBooNE data from the NuMI beam. This beam is 110 mrad off-axis, with a π peak of average ν_μ energy of about 200 MeV and a K peak of about 2 GeV, and a length of 750 m. If an excess of events is observed in this analysis, this rules out mis-estimate of intrinsic ν_e in the Booster Neutrino Beam as the source of the MiniBooNE excess. Results from this study are expected in autumn, 2007.

If the unexplained excess persists after the above studies, then it will be valuable to introduce a detector which can differentiate between electrons and photons. That is the goal of MicroBooNE,⁴⁴ which uses a Liquid argon TPC (LArTPC) detector. This is particularly sensitive at low energies and nearly background-free. Specifically, this detector has a ν_e efficiency $> 80\%$ and rejects photons efficiently through dE/dx deposition in the first ~ 2 cm of the shower. With these qualities the detector can be an order of magnitude smaller in size than MiniBooNE, making quick construction feasible. A proposal for this experiment will be submitted to the Fermilab PAC in autumn 2007.

5.3.2.2. *The NuTeV Anomaly*

Neutrino scattering measurements offer a unique tool to probe the electroweak interactions of the Standard Model (SM). The NuTeV anomaly is a 3σ deviation of $\sin^2 \theta_W$ from the Standard Model prediction.¹⁶² $\sin^2 \theta_W$ parameterizes the mixing between the weak interaction Z boson and the photon in electroweak theory. Deviations of measurements of this parameter, and its partner parameter, ρ , the relative coupling strength of the neutral-to-charged-current interactions, may indicate Beyond-Standard-Model physics. This section also highlights that fact that new neutrino properties may be revealed in TeV-scale interactions at LHC, which has not been addressed previously.

Table 5.6. left and right handed coupling constants.

f	ℓ_f	r_f
e^-	$-\frac{1}{2} + \sin^2 \theta_W$	$\sin^2 \theta_W$
u, c	$\frac{1}{2} - \frac{2}{3} \sin^2 \theta_W$	$-\frac{2}{3} \sin^2 \theta_W$
d, s	$-\frac{1}{2} + \frac{1}{3} \sin^2 \theta_W$	$\frac{1}{3} \sin^2 \theta_W$

The NuTeV experiment represents a departure from the previous train of thought in several ways. NuTeV was a deep inelastic neutrino scattering experiment, and thus is performed at significantly higher energy than the experiments previously discussed. Also, while NuTeV did an oscillation search, it was mainly designed for another purpose: precision measurement of electroweak parameters. We will focus on that purpose here. As a result, this analysis allows new issues related to neutrino physics to be brought into the discussion.

$\sin^2 \theta_W$ in Neutrino Scattering and Other Experiments

In neutrino scattering, the neutral current cross section depends upon $\sin^2 \theta_W$. The dependence is a function of the neutrino flavor and the target. NuTeV was a muon-neutrino-flavor scattering experiment. In this case, the NC cross sections for scattering from a light fermion target are:

$$\frac{d\sigma(\nu_\mu f \rightarrow \nu_\mu f)}{dy} = \frac{G_F^2 s}{\pi} (\ell_f^2 + r_f^2 (1-y)^2) \left(1 + \frac{sy}{M_Z^2}\right)^{-2}, \quad (5.38)$$

$$\frac{d\sigma(\bar{\nu}_\mu f \rightarrow \bar{\nu}_\mu f)}{dy} = \frac{G_F^2 s}{\pi} (\ell_f^2 (1-y)^2 + r_f^2) \left(1 + \frac{sy}{M_Z^2}\right)^{-2}. \quad (5.39)$$

In this equation, f is the type of light fermion: $f = e^-, u, d, s, c$. Several constants appear: G_F is the Fermi constant, M_Z is the mass of the Z . The two kinematic variables are: s , the effective center of mass energy, which depends on the mass of f and y , the inelasticity (see definitions in Sec. 5.1.2). ℓ_f, r_f are left and right handed coupling constants which are given in Table 5.7.

While neutrino scattering has traditionally been a method for measuring $\sin^2 \theta_W$, the “Standard Model Prediction” quoted in literature comes from the very precise measurements made by the LEP and SLD experiments, which have been summarized by the Electroweak Working Group.¹⁶³ $\sin^2 \theta_W$ appears in various measurements from e^+e^- scattering at the Z pole. An example which leads to a highly precise measurement is the “left-right asymmetry” measured from polarized scattering at SLD: $A_{LR} = (\sigma_L - \sigma_R)/(\sigma_L + \sigma_R)$ where σ_L and σ_R refer to the scattering cross sections for left- and right- polarized electrons, respectively. In this case

the asymmetry is given by:

$$A_{LR}(Z^0) \equiv \frac{\left(\frac{1}{2} - \sin^2 \theta_W^{(\text{eff})}\right)^2 - \sin^4 \theta_W^{(\text{eff})}}{\left(\frac{1}{2} - \sin^2 \theta_W^{(\text{eff})}\right)^2 + \sin^4 \theta_W^{(\text{eff})}}, \quad (5.40)$$

When comparing quoted values of the weak mixing angle $\sin^2 \theta_W$, care must be taken because this parameter is defined in various ways. The simplest definition is the “on shell” description:

$$1 - M_W^2/M_Z^2 \equiv \sin^2 \theta_W^{(\text{on-shell})}. \quad (5.41)$$

This is the definition commonly used in neutrino physics. In the discussion which follows, if not explicitly labeled, the on-shell definition for $\sin^2 \theta_W$ is used. A variation on this definition uses the renormalized masses at some arbitrary scale μ which is usually taken to be M_Z :

$$1 - M_W(\mu)^2/M_Z(\mu)^2 \equiv \sin^2 \theta_W^{(\overline{\text{MS}})}. \quad (5.42)$$

However, the LEP experiments used the “effective” weak mixing angle which is related to the vector and axial vector couplings:

$$\frac{1}{4}(1 - g_V^l/g_A^l) \equiv \sin^2 \theta_W^{(\text{eff})}. \quad (5.43)$$

This is what appears in eq. 5.40 above. One must convert between definitions, which have different radiative corrections and renormalization prescriptions, in order to make comparisons.

The parameter $\sin^2 \theta_W$ evolves with Q^2 , the squared 4-momentum transfer of the interaction. Fig. 5.22 illustrates this evolution. The highest Q^2 measurements are from LEP and SLD, with $Q^2 = M_Z^2$. There are several types of experiments, including neutrino experiments, which measure $\sin^2 \theta_W$ with $Q^2 \ll m_Z^2$. NuTeV was performed at $Q^2 = 1$ to 140 GeV^2 , $\langle Q_\nu^2 \rangle = 26 \text{ GeV}^2$, $\langle Q_\nu^2 \rangle = 15 \text{ GeV}^2$. The lowest Q^2 measurements are from studies of atomic parity violation in the nucleus¹⁶⁴ (APV), which arises due to the electroweak interference of the photon and the Z in the boson exchange between the electrons and the nucleus. This samples $Q^2 \sim 0$. At higher Q^2 , there is the result from SLAC E158, a Møller scattering experiment at average $Q^2 = 0.026 \text{ GeV}^2$.¹⁶⁵ Using the measurements at the Z -pole with $Q^2 = M_Z^2$ to fix the value of $\sin^2 \theta_W$, and evolving to low Q^2 , Fig. 5.22¹⁶⁶ shows that APV and SLAC E158 are in agreement with the Standard Model.

NuTeV is strikingly off the prediction of Fig. 5.22. Neutrino scattering may measure a different result because new physics enters the neutrino

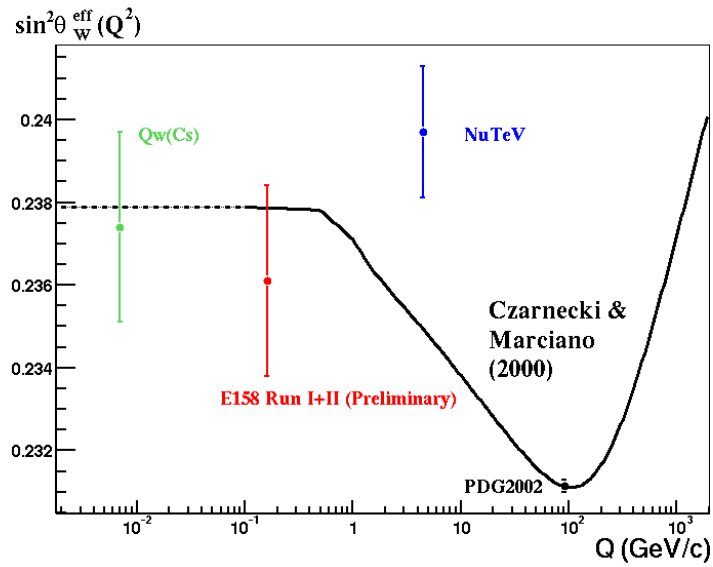


Fig. 5.22. Measurements of $\sin^2 \theta_W$ as a function of Q .¹⁶⁶ The curve shows the Standard Model expectation.

process differently than the other experiments. Compared to the colliders, neutrino physics measures different combinations of couplings. Also neutrino scattering explores new physics through moderate space-like momentum transfer, as opposed to the time-like scattering at the colliders. With respect to the lower energy experiments, the radiative corrections to neutrino interactions allow sensitivity to high-mass particles which are complementary to the APV and Møller-scattering corrections.

The NuTeV Result The NuTeV experiment provides the most precise measurement of $\sin^2 \theta_W$ from neutrino experiments. The measurement relied upon deep inelastic scatter (DIS). It was performed using a “Paschos-Wolfenstein style”¹⁶⁷ analysis which is designed to minimize the systematic errors which come from our understanding of parton distributions and masses.

This method requires separated ν and $\bar{\nu}$ beams. In this case, the following ratios could be formed:

$$R^\nu = \frac{\sigma_{NC}^\nu}{\sigma_{CC}^\nu} \quad (5.44)$$

$$R^{\bar{\nu}} = \frac{\sigma_{NC}^{\bar{\nu}}}{\sigma_{CC}^{\bar{\nu}}} \quad (5.45)$$

$$(5.46)$$

Paschos and Wolfenstein¹⁶⁷ recast these as:

$$R^- = \frac{\sigma_{NC}^\nu - \sigma_{NC}^{\bar{\nu}}}{\sigma_{CC}^\nu - \sigma_{CC}^{\bar{\nu}}} = \frac{R^\nu - rR^{\bar{\nu}}}{1 - r}, \quad (5.47)$$

where $r = \sigma_{CC}^{\bar{\nu}}/\sigma_{CC}^\nu$. In the case of R^- , many systematics cancel to first order. In particular, the quark and antiquark seas for u, d, s , and c , which are less precisely known than the valence quark distributions, will cancel. Charm production only enters through $d_{valence}$ which is Cabbibo suppressed and at high x , thus the error from the charm mass is greatly reduced. One can also form R^+ , but this will have much larger systematic errors, and so the strength of the NuTeV analysis lies in the measurement of R^- .

According to the “Paschos-Wolfenstein” method, an experiment should run in neutrino and antineutrino mode, categorize the events as CC or NC DIS, and then form R^- to extract $\sin^2 \theta_W$. This requires identifying the CC or NC events properly in NuTeV’s iron-scintillator/drift-chamber calorimeter. Most CC DIS events have an exiting muon, which causes a long string of hits in the scintillator and are therefore called “long.” Most NC DIS events are relatively “short” hadronic showers. However, there are exceptions to these rules. A CC event caused by interaction of an intrinsic ν_e in the beam will appear short. An NC shower which contains a pion-decay-in-flight, producing a muon, may appear long. The connection between long vs. short and CC vs. NC must be made via Monte Carlo.

NuTeV measurement is in agreement with past neutrino scattering results, although these have much larger errors. However, the NuTeV result

is in disagreement with the global fits to the electroweak data which give a Standard Model value of $\sin^2\theta_W = 0.2227$.¹⁶²

Explanations In the case of any anomaly, it is best to start with the commonplace explanations. Three explanations for the NuTeV anomaly that are “within the Standard Model” have been proposed: the QCD-order of the analysis, isospin violation, and the strange sea asymmetry. The NuTeV analysis was not performed at a full NLO level. However, the effect of going to NLO on NuTeV can be estimated,¹⁶⁸ and the expected pull is away from the Standard Model. The NuTeV analysis assumed isospin symmetry, that is, $u(x)^p = d(x)^n$ and $d(x)^p = u(x)^n$. Various models for isospin violation have been studied and their pulls range from less than 1σ away from the Standard Model to $\sim 1\sigma$ toward the Standard Model.¹⁶⁹ Variations in the strange sea can either pull the result toward or away from the Standard Model expectation,¹⁶⁹ but not by more than one sigma.

With respect to Beyond-Standard-Model explanations, Chapter 14 of the APS Neutrino Study White Paper on Neutrino Theory² is dedicated to “The Physics of NuTeV” and provides an excellent summary. The discussion presented here is drawn from this source.

The NuTeV measurements of R^ν and $R^{\bar{\nu}}$, the NC-to-CC cross sections, are low compared to expectation. For this to be a Beyond-Standard-Model effect, it therefore requires introduction of new physics that suppresses the NC rate with respect to the CC rate. Two types of models produce this effect and remain consistent with the other electroweak measurements: (1) models which affect only the Z couplings, *e.g.*, the introduction of a heavy Z' boson which interferes with the Standard Model Z ; or (2) models which affect only the neutrino couplings, *e.g.*, the introduction of moderate mass neutral heavy leptons which mix with the neutrino.

Any Z' model invoked to explain NuTeV must selectively suppress NC neutrino scattering, without significantly affecting the other electroweak measurements. This rules out most models, which tend to increase the NC scattering rate. Examples of successful models are those where the Z' couples to $B - 3L_\mu$ ¹⁷⁰ or to $L_\mu - L_\tau$.¹⁷¹

Moderate-mass neutral heavy leptons, *a.k.a.* “neutrissimos,” can also produce the desired effect. Suppression of the coupling comes from inter-generational mixing of heavy states, so that the ν_μ is a mixture:

$$\nu_\mu = (\cos \alpha)\nu_{\text{light}} + (\sin \alpha)\nu_{\text{heavy}}. \quad (5.48)$$

The $Z\nu_\mu\nu_\mu$ coupling is modified by $\cos^2 \alpha$ and the $W\mu\nu_\mu$ coupling is mod-

ified by $\cos \alpha$. Neutrissimos may have masses as light as ~ 100 GeV.¹⁷² These new particles can play the role of the seesaw right-handed neutrinos, as long as one is willing to admit large tuning among the neutrino Yukawa couplings.¹⁷² So this offers an alternative to the GUT-mass heavy neutrino model discussed in sec. 5.3.1.

If neutrissimos exist, they would be expected to show up in other precision experiments. One must avoid the constraints on mixing from $0\nu\beta\beta$ (recall eq. 5.31 to see why these experiments have sensitivity to the mixing). These experiment place a limit of $|U_{e4}|^2$ at less than a few $\times 10^{-5}$ for a 100 GeV right-handed neutrino. Rare pion and tau decays constrain $|U_{\mu 4}|^2$ to be less than 0.004 and $|U_{\tau 4}|^2$ to be less than 0.006, respectively.

Neutrissimos would be produced at LHC, thus neutrino physics can be done at the highest energy scales! However, they may be difficult to observe. One would naturally look for a signal of missing energy. However, neutrissimos will not necessarily decay invisibly; for example one can have $N \rightarrow \ell + W$ and the W may decay to either two jets or a neutrino-charged-lepton pair. Only the latter case has missing energy. This may make them difficult to identify.

If the neutrissimo is a Majorana particle, then these could provide a clue to the mechanism for leptogenesis. The present models of leptogenesis require very high mass scales for the neutral lepton. However, theorists are identifying ways to modify the model to accommodate lower masses.¹⁷³ There also may be a wide mass spectrum for these particles, with one very heavy case that accommodates standard leptogenesis models, while the others have masses in the range observable at LHC.¹⁷⁴

NuSONG and Other Possibilities A new round of precision electroweak measurements can be motivated by the NuTeV anomaly as well as the imminent turn-on of LHC. These measurements are best done using neutrino-electron scattering, because this removes the quark-model related questions discussed in the previous section. Two possible methods for such a measurement are ν_μ scattering with higher statistics, using a NuTeV-style beam, or a $\bar{\nu}_e s$ scattering measurement from a reactor. In either case, to provide a competitive measurement, the error from the best present neutrino-electron scattering measurement, from CHARM II, must be reduced by a factor of five.

The NuSONG (Neutrino Scattering On Glass) Experiment¹⁷⁵ is proposed to run using a ν_μ beam produced by 800 GeV protons on target from the

TeVatron. The plan is to use a design which is inspired by the CHARM II experiment: a target of SiO_2 in one quarter radiation length panels, with proportional tubes or scintillator to allow event reconstruction. The detector will have a 2.6 kton fiducial volume. The major technical challenge of such an experiment is in achieving the required rates from the TeVatron, as $\times 20$ the rate of NuTeV proton delivery is required.

Alternatively, a measurement of the weak mixing angle using anti-neutrinos from reactors may be possible.¹⁷⁶ The weak mixing angle can be extracted from the purely leptonic $\bar{\nu}_e e$ “elastic scatter” (ES) rate, which is normalized using the $\bar{\nu}_e p$ “inverse beta decay” (IBD) events, to reduce the error on the flux. Thus, a hydrocarbon (scintillator oil) based detector, which has free proton targets for the IBD events, is ideal. Gadolinium (Gd) doping is necessary for a high rate of neutron capture, which constitutes the signal for the IBD events. A window in visible energy of 3 to 5 MeV is selected to reduce backgrounds from contaminants in the oil and cosmic-muon-induced isotopes. In this energy range, the dominant contamination comes from the progeny of the uranium and thorium chain. This would clearly be an ambitious, state-of-the-art measurement, but could be done at a new reactor experiment where the detector is in close proximity to the source and had high shielding from cosmic rays.

5.3.3. *Neutrinos and the Cosmos*

Neutrinos are ubiquitous in the universe, and their presence and interactions must be incorporated into astrophysical and cosmological models. Nearly any new neutrino property will have direct consequences in these fields, which must be examined. As an illustrative example, the first discussion considers the impact of introducing of relatively light sterile neutrinos to the theory. Sterile neutrinos with keV-scale masses can explain dark matter as well other astrophysical questions.

As we improve our capability for detecting astrophysical neutrinos, these become a new source of neutrinos for study. The second example is a case in point: the search for ultra-high energy sources of neutrinos. The discovery of such sources would be of great interest to astrophysics, and the particle physics we can do with such a “beam” is remarkable.

While this section concentrates on the unknown, it is interesting to note that the known astrophysical sources of neutrinos are sufficiently intense that these neutrinos are already a possible background to other physics measurements. An example is the case of dark matter searches, which aim

to measure cross sections as small as 10^{-46} cm². These experiments will have to contend with the background from coherent scattering ($\nu + N \rightarrow \nu + N$) of solar neutrinos, which has a cross section of 10^{-39} cm² and which produces a recoil nucleon that is very much like the expected dark matter signal.¹⁷⁷

5.3.3.1. Neutrinos as Dark Matter

From the mid-1980's through mid-90's a 5 eV ν_τ was considered a likely candidate for dark matter. This was the motivation for the Chorus and NOMAD search for $\nu_\mu \rightarrow \nu_\tau$ oscillations in the > 10 eV² range^{178,179} as well as the proposed COSMOS experiment.¹⁸⁰

In the late 90's and early 2000's, two measurements led to a shift in opinion about neutrinos as candidates for dark matter. The first was the Super-K confirmation of ν_μ oscillations. As discussed in sec. 5.2.1.4, the cleanest explanation, which fits within a three-neutrino model, is that this effect is $\nu_\mu \rightarrow \nu_\tau$. Combining this information with the direct limit on the ν_e implied that neutrinos were unlikely to have masses in the 5 to 10 eV range, as required for dark matter. Also, at the same time, studies of the large scale structure of the universe indicated that dark matter must be non-relativistic, or "cold." Relativistic, or "hot dark matter," like neutrinos, would smooth the large scale structure far beyond observations.¹⁸¹

The idea of neutrinos as dark matter candidates fell into disfavor. For some time, the more likely solution was assumed to be WIMPs, Weakly Interacting Massive Particles. The "weak" in this name is somewhat confusing, since it does not refer strictly to the weak interaction – other Beyond-Standard-Model interactions are involved. It is simply meant to say that the interaction rate is very low.

For some time, the lightest supersymmetric particle has been the most favored candidate for the WIMP. However, this is now starting to be questioned, as no evidence for supersymmetry has been observed at colliders.¹⁸² This makes the formulation of the theory more awkward, and SUSY explanations for dark matter have been pushed from the "Minimal Super Symmetric Model" to the "Next-to-Minimal Super Symmetric Model," and even this is challenged.¹⁸³ If supersymmetry does not show up at LHC, then a new explanation for dark matter must be found.

As a result, neutrino models are being reconsidered.^{184–193} The new models involve neutrinos which are mostly sterile, with a very tiny mixing with the light flavors and with keV masses ($0.5 \text{ keV} < m_\nu < 15 \text{ keV}$ and

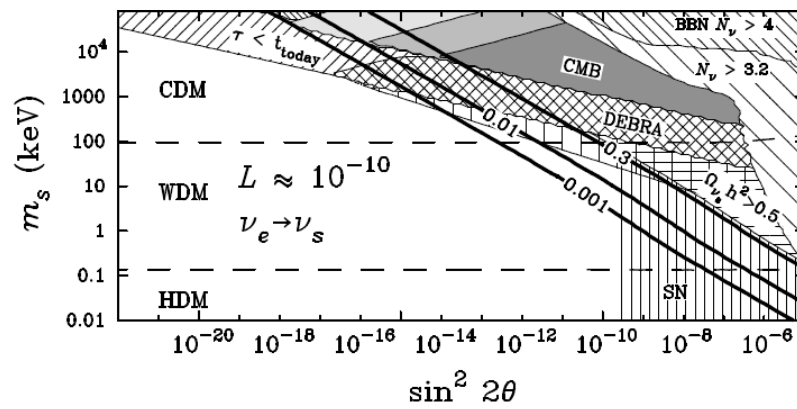


Fig. 5.23. Bounds for $\nu_e \rightarrow \nu_s$ oscillations from astrophysics and cosmology. Allowed regions for neutrino cold, warm and hot dark matter are shown.¹⁸⁷

$\sin^2 2\theta \geq 10^{-12}$) Because of the high mass, they are not relativistic and are regarded as “warm” or “cold.” At high mass, the large scale structure limits are much less stringent. A recent analysis from the Sloan Digital Sky Survey (SDSS) finds that a sterile neutrino mass above 9 keV can reproduce the power spectrum.¹⁹⁴ Only tiny mixing with the active neutrinos is required in order to produce the dark matter. With such small mixings, this model easily evades all accelerator-based bounds on $\nu_e \rightarrow \nu_s$ oscillations. As shown in Fig. 5.23, this model also escapes the cosmological limits on $\nu_e \rightarrow \nu_s$ from the CMB measurements, from Big Bang Nucleosynthesis (BBN), and supernova limits (SN), assuming negligible lepton number asymmetry, L , in the early universe.

Currently the only constraints on keV sterile neutrinos come from X-ray astronomy¹⁹³ which are searching for evidence of radiative decay of the massive neutrino into a lighter state, $\nu_2 \rightarrow \nu_1 + \gamma$. This proceeds through

loop diagrams where the photon is coupling to a W or a charged lepton in the loop.¹⁹⁵ Because this is a 2-body decay, one is searching for a spectral line in the x-ray region. For a Dirac-type sterile neutrinos of mass m_s the decay rate is given by:

$$\Gamma_\gamma(m_s) = 1.36 \times 10^{-29} \text{s}^{-1} \left(\frac{\sin^2 2\theta}{10^{-7}} \right) \left(\frac{m_s}{1 \text{keV}} \right)^5, \quad (5.49)$$

which is clearly tiny, even for a keV scale neutrino. This is important as the dark matter neutrinos must be stable on the scale of the lifetime of the universe. No signal has been observed and the current mass limit, from the Chandra X-ray telescope observations, ranges from >3 to >6 keV depending on model assumptions.

Having motivated a keV-mass sterile state using dark matter, one can explore the consequences in other areas of cosmology and astrophysics. The small mixing allows these neutrinos to evade bounds from big bang nucleosynthesis.¹⁹⁶ Their presence may be beneficial to models of supernova explosions and pulsar kicks, as discussed below.

The existence of these neutrinos may improve the supernova models substantially. The problem faced by most models is that the supernova stalls and fails to explode. As modest increase in neutrino luminosity during the epoch when the stalled bounce shock is being reheated ($t_{\text{pb}} < 1 \text{s}$) will incite the explosion.¹⁹⁷ As the supernova occurs, neutrinos will oscillate and even be affected by MSW resonances. If neutrinos oscillate to a sterile state, then their transport-mean-free-paths become larger. This increases the neutrino luminosity at the neutrino sphere and makes “the difference between a dud and an explosion.”¹⁹⁷

Also, sterile neutrinos in the 1 to 20 keV mass range can also be used to explain the origin of pulsar motion. Pulsars are known to have large velocities, from 100 to 1600 km/s. This is a much higher velocity than an ordinary star which typically has 30 km/s. Pulsars also have very high angular velocities. Apparently, there is some mechanism to give pulsars a substantial “kick” at birth, which sends them off with high translational and rotational velocities. One explanation for the kick is an asymmetric neutrino emission of sterile neutrinos during or moments after the explosion which forms the pulsar.¹⁹⁶ An asymmetry in neutrino emission occurs because the “urca reactions”

$$\nu_e + n \leftrightarrow p + e^-, \quad (5.50)$$

$$\bar{\nu}_e + p \leftrightarrow n + e^+, \quad (5.51)$$

are affected by magnetic fields which trap electrons and positrons. If the neutrinos oscillate to a sterile state, they stream out of the pulsar. If the sterile neutrinos have high mass, they can provide a significant kick. There are a number of solutions, either with standard neutrino oscillations, as described by eq. 5.10 or with an MSW-type resonance. All require a sterile state in the 1 to 20 keV range with very small mixing, compatible with the dark matter scenario described above.

In summary, this is an example of how introducing a new neutrino property, *i.e.* sterile companions to the known neutrinos, can have a major impact on astrophysical models. This is an interesting case in point, because it is unlikely that these neutrinos will be observable in particle physics experiments in the near future. At present, the only detection method is through X-ray emission due to the radiative decay. Thus this is, at the moment, an example of a neutrino property which is entirely motivated and explored in the context of astrophysics.

5.3.3.2. Ultra High Energy Neutrinos

All of the experiments so-far discussed have used neutrino sources in the energy range of a few MeV to many GeV. We do not know how to produce neutrino beams at higher energies. However, nature clearly has high energy acceleration mechanisms, because cosmic rays with energies of 10^8 GeV have been measured. A new generation of neutrino experiments is now looking for neutrinos at these energies and beyond. These include AMANDA,³⁴ ICEcube,¹⁹⁸ Antares,³⁵ and Anita.¹⁹⁹

These experiments make use of the fact that the Earth is opaque to ultra-high energy neutrinos. The apparent weakness of the weak interaction, which is due to the suppression by the mass of the W in the propagator term, is reduced as the neutrino energy increases. Amazingly, when you reach neutrino energies of 10^{17} eV, the Earth becomes opaque to neutrinos. To see this, recalling the kinematic variables defined in sec. 5.1.2, consider the following back-of-the-envelope calculation. For a 10^8 GeV ν , $s = 2ME_\nu = 2 \times 10^8$ GeV². Most interactions occur at low x ; and at these energies $x_{\text{typical}} \sim 0.001$. For neutrino interactions, the average y is 0.5. Therefore, using $Q^2 = sxy$, we find $Q_{\text{typical}}^2 = (2 \times 10^8)(1 \times 10^{-3})(0.5) = 1 \times 10^5$ GeV². The propagator term

goes as

$$\left(\frac{M_W^2}{M_W^2 + Q^2}\right)^2 = \left(\frac{1}{1 + Q^2/M_W^2}\right)^2 \approx \frac{M_W^4}{Q^4}, \quad (5.52)$$

which is approximately 10^{-3} for our “typical” case. The typical cross section $\sigma_{typical}$ is:

$E \times (\sigma_{tot}/E) \times (\text{prop term}) = 10^8(\text{GeV})(0.6 \times 10^{-38} \text{cm}^2/\text{GeV})10^{-3} = 0.6 \times 10^{-33} \text{cm}^2$. From this we can extract the interaction length, λ_0 , on iron, by scaling from hadronic interactions, which tells us that at 30 mb ($= 0.3 \times 10^{-25} \text{cm}^2$), $1\lambda_0 \sim 10 \text{cm}$. This implies that λ_0 for our very high energy ν s is $\approx 5 \times 10^3 \text{km}$. However, the Earth is a few $\times 10^4 \text{km}$. Thus all of the neutrinos interact; the Earth is opaque to them.

This opens up the opportunity to instrument the Earth and use it as a neutrino target. One option is to choose a transparent region of the Earth, ice or water, and instrument it like a traditional neutrino detector. This has been the design chosen by AMANDA, ICECube and Antares, which use phototubes to sense the Cerenkov light produced when charged particles from neutrino interactions traverse the material. The largest of these detectors are on the order of $(1 \text{km})^3$ of instrumented area. The second method exploits the Askaryan effect²⁰⁰ in electromagnetic showers. Electron and positron scattering in matter have different cross sections. As the electromagnetic shower develops, this difference leads to a negative charge asymmetry, inducing strong coherent Cerenkov radiation in the radio range. The pulse has unique and easy-to-distinguish broadband (0.2 - 1.1 GHz) spectral and polarization properties which can be received by detecting antennas launched above the target area. In ice, the radio attenuation length is 1 km. The Anita Experiment, which uses such a detector, can view $2 \times 10^6 \text{km}^3$ of volume. This makes it by far the world’s largest tonnage experiment.

Neutrinos with energies above 10^4GeV have yet to be observed. However, they are expected to accompany ultra high energy cosmic rays, which have been observed. Nearly all potential sources of ultra-high energy cosmic rays are predicted to produce protons, neutrinos, and gamma rays at roughly comparable levels. Ultra high energy protons, which have been observed by the HiRes²⁰¹ and Auger²⁰² experiments are guaranteed sources of neutrinos through the Greisen-Zatsepin-Kuzmin (GZK) interaction. In this effect, protons above $E_{GZK} = 6 \times 10^{10} \text{GeV}$ scatter from the cosmic microwave background: $p\gamma \rightarrow \Delta^+ \rightarrow n\pi^+$. This degrades the energy of protons above E_{GZK} , leading to an apparent cutoff in the flux called the

“GZK cutoff.” There are several Δ resonances and the CMB photons have an energy distribution, so the cutoff is not sharp. But it has been clearly observed by both HiRes and Auger.²⁰³ As a result, ultra-high energy pions are produced and these must decay to ultra-high-energy neutrinos. There may be other, more exotic mechanisms for producing an ultra-high energy flux, possibly with energies beyond the GZK cutoff. Since, unlike the protons, these neutrinos do not interact with the cosmic microwave background, they can traverse long distances and can be messengers of distant point sources.

There many reviews of the exotic physics one can do with ultra high energy neutrino interactions. The opportunities include²⁰⁴ gravitational lensing of neutrinos, the search for bumps or steps in the NC/CC ratio, the influence of new physics on neutrino oscillations at high energies, the search for neutrino decays, neutrino interaction with dark matter WIMPs, and the annihilation of the ultra high energy neutrinos by the cosmic neutrino background. This final example is interesting because significant limits have been set by Anita-lite, a small prototype for Anita that flew only 18.4 days. This illustrates the power of even a small experiment entering an unexplored frontier of particle physics.

The 1 eV mass neutrino implied by the LSND anomaly could be a candidate for the source of the ultra-high energy cosmic rays observed on Earth.²⁰⁵ This neutrino, if produced at ultra-high energies, could annihilate on the cosmic neutrino background producing a “Z-burst” of ultra high energy hadrons. This was offered as an explanation for ultra-high energy cosmic which were observed by the AGASA experiment.²⁰⁶ Scaling from the AGASA rate, a prediction for the flux of ultra-high neutrinos in the energy range of $10^{18.5} < E_\nu < 10^{23.5}$ eV for Z-burst models was made.^{207,208} Based on this flux, Anita-lite was predicted to see between 5 and 50 events at >99% CL. During its short run, this prototype detector observed no events in the energy range and therefore could definitively rule out this model.²⁰⁹ Shortly thereafter, the AGASA events were shown to be due to energy miscalibration.²¹⁰

5.4. Conclusions

The goal of this review was to sketch out the present questions in neutrino physics, and discuss the experiments that can address them. Along the way, I have highlighted the experimental techniques and challenges. I have also tried to briefly touch on technological advances expected in the near future.

This text followed the structure of the set of lectures entitled “Neutrino Experiments,” given at the 2006 TASI Summer School.

Neutrino physics is an amalgam of astrophysics, cosmology, nuclear physics, and particle physics, making the field diverse and exciting, but hard to review comprehensively. In this paper, I have tried to touch on examples which are particularly instructive and have been forced to leave out a wide range of other interesting points. What should be clear, however, is that the recent discoveries by neutrino experiments have opened up a wide range of interesting questions and opportunities. This promises to be a rich field of research for both theorists and experimentalists for years to come.

I wish to thank A. Aguilar-Arevalo, G. Karagiorgi, B. Kayser, P. Nienaber, J. Spitz, and E. Zimmerman for their suggestions concerning this text.

References

1. <https://www.interactions.org/cms/?pid=1009695>
2. R.N. Mohapatra, *et al.*, hep-ph/050213v2, 2005.
3. <http://neutrinooscillation.org/>
4. D. Decamp, *et al.*, CERN-EP/89-169, Phys.Lett.B235:399, 1990.
5. H. Band, *et al.*, SLAC-PUB-4990, published in the Proceedings of the Fourth Family of Quarks ,and Leptons, Santa Monica, CA, Feb 23-25, 1989.
6. <http://fn872.fnal.gov/>
7. C.S. Wu, *et al.* Phys. Rev. 105, 1413, 1957.
8. P. Lipari, Nucl. Phys. Proc. Suppl. **112**, 274 (2002) [arXiv:hep-ph/0207172].
9. D. Casper, Nucl. Phys. Proc. Suppl. 112:161, 2002.
10. <http://www-boone.fnal.gov>.
11. <http://www-sciboone.fnal.gov/>
12. <http://minerva.fnal.gov/>
13. <http://www.sns.ias.edu/~jnb>.
14. R. Davis, Prog. Part. Nucl. Phys. **32**, 13 (1994); B. T. Cleveland *et al.*, Astrophys. J. **496**, 505 (1998).
15. J. N. Abdurashitov *et al.* [SAGE Collaboration], J. Exp. Theor. Phys. **95**, 181 (2002) [Zh. Eksp. Teor. Fiz. **122**, 211 (2002)] [arXiv:astro-ph/0204245].
16. W. Hampel *et al.* [GALLEX Collaboration], Phys. Lett. B **447**, 127 (1999).
17. K. Eguchi *et al.* [KamLAND Collaboration], Phys. Rev. Lett. **92**, 071301 (2004) [arXiv:hep-ex/0310047].

18. C. H. Albright *et al.* [Neutrino Factory/Muon Collider Collaboration], arXiv:physics/0411123.
19. See, for example, S. E. Kopp, Phys. Rept. **439**, 101 (2007) [arXiv:physics/0609129].
20. D.E. Groom *et al.*, The European Physical Journal C15: 1, 2000.
21. G. D. Barr, T. K. Gaisser, P. Lipari, S. Robbins and T. Stanev, Phys. Rev. D **70**, 023006 (2004) [arXiv:astro-ph/0403630].
22. J. Hosaka *et al.* [Super-Kamioke Collaboration], Phys. Rev. D **73**, 112001 (2006) [arXiv:hep-ex/0508053].
23. H. Back *et al.*, arXiv:hep-ex/0412016.
24. G. D. Barr, T. K. Gaisser, S. Robbins and T. Stanev, Phys. Rev. D **74**, 094009 (2006) [arXiv:astro-ph/0611266].
25. M. Apollonio *et al.*, Eur. Phys. J. C **27**, 331 (2003) [arXiv:hep-ex/0301017].
26. T. Araki *et al.* [KamLAND Collaboration], [arXiv:hep-ex/0406035].
27. C. Athanassopoulos *et al.* [LSND Collaboration], Nucl. Instrum. Meth. A **388**, 149 (1997) [arXiv:nucl-ex/9605002].
28. <http://pupgg.princeton.edu/borexino/welcome.html>
29. K. Nakamura [KamLAND Collaboration], AIP Conf. Proc. **721**, 12 (2004).
30. C. Kraus [SNO+ Collaboration], Prog. Part. Nucl. Phys. **57**, 150 (2006).
31. Karsten Heeger, private communication.
32. E. Church *et al.* [BooNE Collaboration], "A proposal for an experiment to measure muon-neutrino \rightarrow electron-neutrino oscillations and muon-neutrino disappearance at the Fermilab Booster: BooNE," FERMILAB-PROPOSAL-0898;
33. <http://www-sk.icrr.u-tokyo.ac.jp/sk/index.html>
34. <http://amanda.berkeley.edu/>
35. <http://antares.in2p3.fr/>
36. <http://www-numi.fnal.gov/>
37. <http://www-e815.fnal.gov/>
38. S. Yamamoto *et al.*, IEEE Trans. Nucl. Sci. **52**, 2992 (2005).
39. A. Pla-Dalmau, A. D. Bross, V. V. Rykalin and B. M. Wood [MINERvA Collaboration],
40. <http://www-nova.fnal.gov/>
41. A. Curioni, *et al.*, hep-ex/0603009.
42. S. Amerio, *et al.*, NIM A527: 329, 2004.
43. <http://t962.fnal.gov/>
44. http://www.fnal.gov/directorate/Longrange/Steering_Public/community_letters.html, see letter 15: "MicroBooNE - Fleming and Willis," June 12, 2007
45. http://www.fnal.gov/directorate/Longrange/Steering_Public/community_letters.html, see letter 14: "Neutrino Expt with 5kton LAr TPC" Fleming and Rameika, June 12, 2007; D. Finley *et al.*,
46. L. Wolfenstein, Phys. Rev. D17, 2369 (1978); D20, 2634 (1979); S. P. Mikheyev and A. Yu. Smirnov, Yad. Fiz. 42, 1441 (1985) [Sov. J. Nucl. Phys. 42, 913 (1986)]; Nuovo Cimento 9C, 17 (1986).

47. G. J. Feldman and R. D. Cousins, Phys. Rev. D **57**, 3873 (1998) [arXiv:physics/9711021].
48. T. Schwetz, Acta Phys. Polon. B **36**, 3203 (2005) [arXiv:hep-ph/0510331].
49. B. Kayser, "Neutrino Mass, Mixing, and Flavor Change," available from the PDG website: http://pdg.lbl.gov/2007/reviews/contents_sports.html, W.-M. Yao, *et al.*, J. Phys. G **33**, 1 (2006).
50. Y. Totsuka, Nucl. Phys. A663, 218 (2000); Y. Fukuda, *et al.* Phys. Rev. Lett. **81**, 1562 (1998)
51. D. Casper *et al.*, Phys. Rev. Lett. **66**, 2561 (1991); R. Becker-Szendy *et al.*, Phys. Rev. Lett. **69**, 1010 (1992).
52. E. Kearns, talk presented at Neutrino 2004.
53. Y. Fukuda *et al.* [Super-Kamiokande Collaboration], Phys. Lett. B **433**, 9 (1998) [arXiv:hep-ex/9803006]; Phys. Lett. B **436**, 33 (1998) [arXiv:hep-ex/9805006]; Phys. Rev. Lett. **81**, 1562 (1998) [arXiv:hep-ex/9807003]; Phys. Rev. Lett. **82**, 2644 (1999) [arXiv:hep-ex/9812014]; Phys. Lett. B **467**, 185 (1999) [arXiv:hep-ex/9908049]; Y. Ashie *et al.* [Super-Kamiokande Collaboration], Phys. Rev. D **71**, 112005 (2005) [arXiv:hep-ex/0501064].
54. S. H. Ahn *et al.* [K2K Collaboration], Phys. Lett. B **511**, 178 (2001) [arXiv:hep-ex/0103001]; Phys. Rev. Lett. **90**, 041801 (2003) [arXiv:hep-ex/0212007]; Phys. Rev. D **74**, 072003 (2006) [arXiv:hep-ex/0606032].
55. D. G. Michael *et al.* [MINOS Collaboration], [arXiv:hep-ex/0607088].
56. N. Saoulidou for the MINOS Collaboration, <http://theory.fnal.gov/jetp/> July 19, 2007.
57. A. Habig [Super-Kamiokande Collaboration], arXiv:hep-ex/0106025.
58. <http://www.cern.ch/opera>.
59. J. Marteau [for the OPERA collaboration], arXiv:0706.1699 [hep-ex].
60. E. G. Adelberger *et al.*, "Solar Fusion Cross Sections," To be published in Rev. Mod. Phys., Oct. 1998, astro-ph/9805121.
61. For example, J. Christensen-Dalsgaard *et al.*, Science **272** 1286 (1996).
62. For example, Castellani *et al.*, Nucl. Phys. Proc. Suppl. **70** 301 (1998).
63. <http://www.sno.phy.queensu.ca>.
64. B. Aharmim *et al.* [SNO Collaboration], arXiv:nucl-ex/0610020.
65. J. N. Bahcall, M. H. Pinsonneault and S. Basu, Astrophys. J. **555**, 990 (2001) [arXiv:astro-ph/0010346].
66. T. Araki *et al.* [KamLAND Collaboration], Phys. Rev. Lett. **94**, 081801 (2005) [arXiv:hep-ex/0406035].
67. T. Schwetz, Phys. Scripta **T127**, 1 (2006) [arXiv:hep-ph/0606060].
68. H. S. Goh, R. N. Mohapatra and S. P. Ng, Phys. Rev. D **68**, 115008 (2003) [arXiv:hep-ph/0308197].
69. T. Asaka, W. Buchmuller and L. Covi, Phys. Lett. B **563**, 209 (2003) [arXiv:hep-ph/0304142].
70. K. S. Babu, J. C. Pati and F. Wilczek, Nucl. Phys. B **566**, 33 (2000) [arXiv:hep-ph/9812538].
71. C. H. Albright and S. M. Barr, Phys. Rev. D **64**, 073010 (2001) [arXiv:hep-ph/0104294].

- 72. T. Blazek, S. Raby and K. Tobe, Phys. Rev. D **62**, 055001 (2000) [arXiv:hep-ph/9912482].
- 73. G. G. Ross and L. Velasco-Sevilla, Nucl. Phys. B **653**, 3 (2003) [arXiv:hep-ph/0208218].
- 74. S. Raby, Phys. Lett. B **561**, 119 (2003) [arXiv:hep-ph/0302027].
- 75. R. Kitano and Y. Mimura, Phys. Rev. D **63**, 016008 (2001) [arXiv:hep-ph/0008269].
- 76. N. Maekawa, arXiv:astro-ph/0010559.
- 77. M. C. Chen and K. T. Mahanthappa, Phys. Rev. D **68**, 017301 (2003) [arXiv:hep-ph/0212375].
- 78. M. Bando and M. Obara, Prog. Theor. Phys. **109**, 995 (2003) [arXiv:hep-ph/0302034].
- 79. W. Buchmuller and D. Wyler, Phys. Lett. B **521**, 291 (2001) [arXiv:hep-ph/0108216].
- 80. P. H. Frampton and R. N. Mohapatra, JHEP **0501**, 025 (2005) [arXiv:hep-ph/0407139].
- 81. W. Grimus and L. Lavoura, JHEP **0107**, 045 (2001) [arXiv:hep-ph/0105212].
- 82. W. Grimus and L. Lavoura, Phys. Lett. B **572**, 189 (2003) [arXiv:hep-ph/0305046].
- 83. W. Grimus, A. S. Joshipura, S. Kaneko, L. Lavoura and M. Tanimoto, JHEP **0407**, 078 (2004) [arXiv:hep-ph/0407112].
- 84. M. C. Chen and K. T. Mahanthappa, arXiv:hep-ph/0409165.
- 85. I. Aizawa, M. Ishiguro, T. Kitabayashi and M. Yasue, Phys. Rev. D **70**, 015011 (2004) [arXiv:hep-ph/0405201].
- 86. R. N. Mohapatra, Pramana **63**, 1295 (2004).
- 87. S. Antusch and S. F. King, Nucl. Phys. B **705**, 239 (2005) [arXiv:hep-ph/0402121].
- 88. S. Antusch and S. F. King, Phys. Lett. B **591**, 104 (2004) [arXiv:hep-ph/0403053].
- 89. W. Rodejohann and Z. z. Xing, Phys. Lett. B **601**, 176 (2004) [arXiv:hep-ph/0408195].
- 90. K. S. Babu, E. Ma and J. W. F. Valle, Phys. Lett. B **552**, 207 (2003) [arXiv:hep-ph/0206292].
- 91. T. Ohlsson and G. Seidl, Nucl. Phys. B **643**, 247 (2002) [arXiv:hep-ph/0206087].
- 92. S. F. King and G. G. Ross, Phys. Lett. B **574**, 239 (2003) [arXiv:hep-ph/0307190].
- 93. Q. Shafi and Z. Tavartkiladze, Phys. Lett. B **594**, 177 (2004) [arXiv:hep-ph/0401235].
- 94. R. N. Mohapatra, JHEP **0410**, 027 (2004) [arXiv:hep-ph/0408187].
- 95. M. Bando, S. Kaneko, M. Obara and M. Tanimoto, Phys. Lett. B **580**, 229 (2004) [arXiv:hep-ph/0309310].
- 96. M. Honda, S. Kaneko and M. Tanimoto, JHEP **0309**, 028 (2003) [arXiv:hep-ph/0303227].
- 97. R. F. Lebed and D. R. Martin, Phys. Rev. D **70**, 013004 (2004) [arXiv:hep-ph/0312219].

98. A. Ibarra and G. G. Ross, Phys. Lett. B **575**, 279 (2003) [arXiv:hep-ph/0307051].
99. P. F. Harrison and W. G. Scott, Phys. Lett. B **594**, 324 (2004) [arXiv:hep-ph/0403278].
100. P. H. Frampton, S. L. Glashow and T. Yanagida, Phys. Lett. B **548**, 119 (2002) [arXiv:hep-ph/0208157].
101. A. de Gouvea and H. Murayama, Phys. Lett. B **573**, 94 (2003) [arXiv:hep-ph/0301050].
102. R. N. Mohapatra, M. K. Parida and G. Rajasekaran, Phys. Rev. D **69**, 053007 (2004) [arXiv:hep-ph/0301234].
103. R. Arnowitt, B. Dutta and B. Hu, Nucl. Phys. B **682**, 347 (2004) [arXiv:hep-th/0309033].
104. M. G. Albrow *et al.*, arXiv:hep-ex/0509019.
105. <http://doublechooz.in2p3.fr/>
106. <http://dayawane.ihep.ac.cn/>
107. K. Assamagan, *et al.*, Phys.Rev.D53:6065, 1996.
108. B. Jeckelman, *et al.*, PL B3555 326, 1994.
109. Barate, *et al.*, EPJ C2 395, 1998.
110. C. Kraus *et al.*, Eur. Phys. J. C **40**, 447 (2005) [arXiv:hep-ex/0412056].
111. V. M. Lobashev, *et al.*, Phys.Atom.Nucl.63: 962, 2000.
112. J. Bonn, *et al.*, Phys. Atom. Nucl.63:969, 2000.
113. W. Stoeffl, *et al.*, PRL 75: 3237, 1995.
114. C. Ching, *et al.*, Int. Journ Mod. Phys. A10: 2841, 1995
115. E. Holzschuh, *et al.*, Phys. Lett., B287: 381, 1992.
116. H. Kawakami, *et al.*, Phys. Lett., B256: 105, 1991.
117. H. Robertson, *et al.*, Phys.Rev.Lett.67: 957, 1991; H. Robertson, PR D33: R6, 1991.
118. <http://www-ik.fzk.de/katrin/index.html>
119. R. Bionta, *et al.*, PRL 58: 1494, 1987.
120. K. Hirata, *et al.*, PRL 58: 1490, 1987.
121. S. Hannestad, Prog. Part. Nucl. Phys. **57**, 309 (2006) [arXiv:astro-ph/0511595].
122. J.F. Beacom, N. F. Bell, S. Dodelson, astro-ph/0404585; Z. Chacko, L. J. Hall, S. J. Oliver, M. Perelstein, hep-ph/0405067; K. Abazajian, N. F. Bell, G. M. Fuller and Y. Y. Y. Wong, astro-ph/0410175.
123. A. Alessandrello, *et al.*, Phys. Lett. B486: 13, 2000; L. DeBraekelee, *et al.*, Phys. Atom Nucl 63:1214, 2000; R. Arnold, *et al.*, Nucl. Phys. A678:341, 2000; M. Alston-Garnjost, *et al.*, PR C55: 474, 1997; A. DeSilva, *et al.*, PR C56:2451, 1997; M. Gunther, *et al.*, PR D55:54, 1997; Arnold, *et al.*, Z. Phys. C72: 239, 1996; A. Balysh, *et al.*, PRL 77:5186, 1996.
124. A good discussion of GUT motivation for the sea-saw model appears in Kayser, Gibrat-Debu, and Perrier, *The Physics of Massive Neutrinos*, World Scientific Lecture Notes in Physics, 25, World Scientific Publishing, 1989.
125. V. A. Rodin, A. Faessler, F. Simkovic and P. Vogel, arXiv:nucl-th/0503063.
126. F. Simkovic, G. Pantis, J. D. Vergados and A. Faessler, Phys. Rev. C **60**, 055502 (1999) [arXiv:hep-ph/9905509].

127. M. Aunola and J. Suhonen, Czech. J. Phys. **48**, 145 (1998); M. Aunola and J. Suhonen, Czech. J. Phys. **48**, 145 (1998).
128. S. Stoica and H. V. Klapdor-Kleingrothaus, Nucl. Phys. A **694**, 269 (2001).
129. R. Arnold *et al.* [NEMO Collaboration], Phys. Rev. Lett. **95**, 182302 (2005) [arXiv:hep-ex/0507083].
130. R. Arnold *et al.* [the NEMO Collaboration], JETP Lett. **80**, 377 (2004) [Pisma Zh. Eksp. Teor. Fiz. **80**, 429 (2004)] [arXiv:hep-ex/0410021].
131. O. Cremonesi *et al.* [CUORICINO Collaboration], Phys. Atom. Nucl. **69** (2006) 2083.
132. H. V. Klapdor-Kleingrothaus, I. V. Krivosheina, A. Dietz and O. Chkvorets, Phys. Lett. B **586**, 198 (2004) [arXiv:hep-ph/0404088].
133. S. Schonert *et al.* [GERDA Collaboration], Phys. Atom. Nucl. **69**, 2101 (2006).
134. <http://crio.mib.infn.it/wigmi/pages/cuore.php>
135. <http://nemo.in2p3.fr/supernemo/>
136. <http://0-www-project.slac.stanford.edu.ilsprod.lib.neu.edu/exo/>
137. <http://majorana.pnl.gov/>
138. M. Nomachi *et al.*, Nucl. Phys. Proc. Suppl. **138**, 221 (2005).
139. C. Walter, Talk given at NuINT07, <https://indico.fnal.gov/conferenceOtherViews.py?view=standard&confId=804>, Session 1.
140. D. S. Ayres *et al.* [NOvA Collaboration], arXiv:hep-ex/0503053.
141. <http://jnusrv01.kek.jp/public/t2k/>
142. V. Barger *et al.*, arXiv:0705.4396 [hep-ph].
143. V. Barger, P. Huber, D. Marfatia and W. Winter, arXiv:hep-ph/0703029.
144. V. Barger, P. Huber, D. Marfatia and W. Winter, arXiv:hep-ph/0703029.
145. A. B. Balantekin, AIP Conf. Proc. **847**, 128 (2006) [arXiv:hep-ph/0601113];
146. A. Aguilar *et al.*, Phys. Rev. D **64**
147. B. Armbruster *et al.*, Phys. Rev. D **65** (2002) 112001.
148. B. Achkar *et al.*, Nucl. Phys. B **434** (1995) 503.
149. E. D. Church, K. Eitel, G. B. Mills,
150. B.H.J. McKellar, *et al.* hep-ph/0106121; R.N. Mohapatra, Phys. Rev. D **64** 091301, 2001; hep-ph/0107264; A. Ioannisian and J.W.F. Valle, Phys. Rev. D **63** 073002, 2001; E. Ma, G. Rajasekaran, and U. Sarkar, Phys. Lett. B **495** 363-368, 2000; hep-ph/0006340; Z. Berezhiani and R. Mohapatra, Phys. Rev. D **52** 6607, 1995; R. Fardon, A.E. Nelson, and N. Weiner, arXiv:astro-ph/0309800.
151. M. Sorel, J. Conrad, and M. Shaevitz, Phys. Rev. D **70**:073004,2004, hep-ph/0305255.
152. P. Astier, *et al.* Phys. Lett. B **570**:19, 2003; hep-ex/0306037.
153. F. Dydak *et al.*, Phys. Lett. B **134** 281, 1984..
154. I.E. Stockdale *et al.*, Phys. Rev. Lett. **52**, 1384 (1984); Z. Phys. C **27**, 53 (1985).
155. G. Karagiorgi, A. Aguilar-Arevalo, J. M. Conrad, M. H. Shaevitz, K. Whisnant, M. Sorel and V. Barger, Phys. Rev. D **75**, 013011 (2007) [arXiv:hep-ph/0609177].

156. A. Aguilar-Arevalo, *et al.*, paper in preparation. See also talk by J. Link, NuInt07.
157. M. Maltoni and T. Schwetz, arXiv:0705.0107 [hep-ph].
158. Paper in preparatuon, See talk at NuFact07 website: <http://fphy.hep.okayama-u.ac.jp/nufact07/>
159. T. Katori, A. Kostelecky and R. Tayloe, Phys. Rev. D **74**, 105009 (2006) [arXiv:hep-ph/0606154].
160. H. Pas, S. Pakvasa and T. J. Weiler, AIP Conf. Proc. **903**, 315 (2007) [arXiv:hep-ph/0611263].
161. X. Q. Li, Y. Liu and Z. T. Wei, arXiv:0707.2285 [hep-ph].
162. G. P. Zeller *et al.* Phys. Rev. Lett., **88** 091802, 2002.
163. <http://lepewwg.web.cern.ch/LEPEWWG/>
164. S. C. Bennett and Carl E. Wieman, Phys. Rev. Lett., **82** 2484–2487, 1999.
165. P. L. Anthony *et al.* [SLAC E158 Collaboration], Phys. Rev. Lett. **95**, 081601 (2005) [arXiv:hep-ex/0504049].
166. <http://www.slac.stanford.edu/exp/e158/>
167. E. A. Paschos and L. Wolfenstein, Phys. Rev. D **7**, 91 (1973).
168. K. S. McFarland and S. O. Moch, arXiv:hep-ph/0306052; S. Kretzer and M. H. Reno, Phys. Rev. D **69**, 034002 (2004) [arXiv:hep-ph/0307023]; B. A. Dobrescu and R. K. Ellis, Phys. Rev. D **69**, 114014 (2004) [arXiv:hep-ph/0310154].
169. M. Gluck, P. Jimenez-Delgado and E. Reya, arXiv:hep-ph/0501169; F. M. Steffens and K. Tsushima, Phys. Rev. D **70**, 094040 (2004) [arXiv:hep-ph/0408018]; J. T. Londergan and A. W. Thomas, arXiv:hep-ph/0407247; A. D. Martin, R. G. Roberts, W. J. Stirling and R. S. Thorne, Eur. Phys. J. C **39**, 155 (2005) [arXiv:hep-ph/0411040].
170. S. Davidson, J. Phys. G **29**, 2001 (2003) [arXiv:hep-ph/0209316].
171. E. Ma, D. P. Roy and S. Roy, Phys. Lett. B **525**, 101 (2002) [arXiv:hep-ph/0110146].
172. A. de Gouvea, arXiv:0706.1732 [hep-ph].
173. N. Sahu and U. A. Yajnik, Phys. Rev. D **71**, 023507 (2005) [arXiv:hep-ph/0410075].
174. A. de Gouvea, J. Jenkins and N. Vasudevan, Phys. Rev. D **75**, 013003 (2007) [arXiv:hep-ph/0608147].
175. http://www.fnal.gov/directorate/Longrange/Steering_Public/community_letters.html, see letter 3: “Precision Neutrino Scattering at the TeVatron - Conrad and Fisher,” June 12, 2007. An expression of Interest is in preparation.
176. J. M. Conrad, J. M. Link and M. H. Shaevitz, Phys. Rev. D **71**, 073013 (2005) [arXiv:hep-ex/0403048].
177. J. Monroe and P. Fisher, arXiv:0706.3019 [astro-ph].
178. E. Eskut *et al.* [CHORUS Collaboration], Phys. Lett. B **497**, 8 (2001).
179. P. Astier *et al.* [NOMAD Collaboration], Nucl. Phys. B **611**, 3 (2001) [arXiv:hep-ex/0106102].
180. K. Kodama *et al.*, ‘Muon-neutrino to tau-neutrino oscillations: Proposal,’ FERMILAB-PROPOSAL-0803.

181. S. Bonometto, *New Astron. Rev.* **43**, 169 (1999).
182. M. Carena, D. Hooper and A. Vallinotto, *Phys. Rev. D* **75**, 055010 (2007) [arXiv:hep-ph/0611065]; D. Hooper and A. M. Taylor, *JCAP* **0703**, 017 (2007) [arXiv:hep-ph/0607086].
183. D. G. Cerdeno, E. Gabrielli, D. E. Lopez-Fogliani, C. Munoz and A. M. Teixeira, *JCAP* **0706**, 008 (2007) [arXiv:hep-ph/0701271].
184. S. Colombi, S. Dodelson and L. M. Widrow, *Astrophys. J.* **458**, 1 (1996) [arXiv:astro-ph/9505029]; S. Dodelson and L. M. Widrow, *Phys. Rev. Lett.* **72**, 17 (1994) [arXiv:hep-ph/9303287].
185. T. Asaka, M. Shaposhnikov and A. Kusenko, *Phys. Lett. B* **638**, 401 (2006) [arXiv:hep-ph/0602150].
186. X. D. Shi and G. M. Fuller, *Phys. Rev. Lett.* **83**, 3120 (1999) [arXiv:astro-ph/9904041].
187. K. Abazajian, G. M. Fuller and M. Patel, *Phys. Rev. D* **64**, 023501 (2001) [arXiv:astro-ph/0101524].
188. A. D. Dolgov and S. H. Hansen, arXiv:hep-ph/0103118.
189. A. D. Dolgov and S. H. Hansen, arXiv:hep-ph/0103118.
190. K. Abazajian, *Phys. Rev. D* **73**, 063506 (2006) [arXiv:astro-ph/0511630].
191. P. L. Biermann and A. Kusenko, *Phys. Rev. Lett.* **96**, 091301 (2006) [arXiv:astro-ph/0601004].
192. K. Abazajian and S. M. Koushiappas, *Phys. Rev. D* **74**, 023527 (2006) [arXiv:astro-ph/0605271].
193. K. N. Abazajian, M. Markevitch, S. M. Koushiappas and R. C. Hickox, *Phys. Rev. D* **75**, 063511 (2007) [arXiv:astro-ph/0611144].
194. P. McDonald, *et al.*, *Astrophys. J. Suppl.* **163**, 80 (2006), astro-ph/0405013.
195. P. B. Pal and L. Wolfenstein, *Phys. Rev. D* **25**, 766 (1982).
196. G. M. Fuller, A. Kusenko, I. Mocioiu and S. Pascoli, *Phys. Rev. D* **68**, 103002 (2003) [arXiv:astro-ph/0307267].
197. J. Hidaka and G. M. Fuller, *Phys. Rev. D* **74**, 125015 (2006) [arXiv:astro-ph/0609425].
198. <http://icecube.wisc.edu/>
199. <http://amanda.uci.edu/~anita/>
200. G. A. Askaryan, *JETP Lett.* **50**, 478 (1989) [*Pisma Zh. Eksp. Teor. Fiz.* **50**, 446 (1989)].
201. S. Westerhoff [HiRes Collaboration], *AIP Conf. Proc.* **698**, 370 (2004).
202. <http://www.auger.org/>
203. R. Abbasi *et al.* [HiRes Collaboration], arXiv:astro-ph/0703099.
204. C. Quigg, arXiv:astro-ph/0603372.
205. T. J. Weiler, *Astropart. Phys.* **11**:303 (1999).
206. <http://www.akeno.icrr.u-tokyo.ac.jp/AGASA/>
207. Z. Fodor, S. D. Katz and A. Ringwald, arXiv:hep-ph/0210123.
208. O. Kalashev, G. Gelmini and D. Semikoz, arXiv:0706.3847 [astro-ph].
209. S. W. Barwick *et al.* [ANITA Collaboration], *Phys. Rev. Lett.* **96**, 171101 (2006) [arXiv:astro-ph/0512265].
210. B. M. Connolly, S. Y. BenZvi, C. B. Finley, A. C. O'Neill and S. Westerhoff, *Phys. Rev. D* **74**, 043001 (2006) [arXiv:astro-ph/0606343].